



## Durham E-Theses

---

### *Interfacial properties of fibre reinforced thermo-plastics*

Naqui, Syed Imtiaz

#### How to cite:

---

Naqui, Syed Imtiaz (1992) *Interfacial properties of fibre reinforced thermo-plastics*, Durham theses, Durham University. Available at Durham E-Theses Online: <http://etheses.dur.ac.uk/6069/>

#### Use policy

---

The full-text may be used and/or reproduced, and given to third parties in any format or medium, without prior permission or charge, for personal research or study, educational, or not-for-profit purposes provided that:

- a full bibliographic reference is made to the original source
- a [link](#) is made to the metadata record in Durham E-Theses
- the full-text is not changed in any way

The full-text must not be sold in any format or medium without the formal permission of the copyright holders.

Please consult the [full Durham E-Theses policy](#) for further details.

**INTERFACIAL PROPERTIES OF FIBRE  
REINFORCED THERMO-PLASTICS**

**This thesis presented for the degree of**

**Master of Science**

**of the**

**UNIVERSITY OF DURHAM  
School of Engineering and Computer Science**

**by**

**SYED IMTIAZ NAQUI**

The copyright of this thesis rests with the author.  
No quotation from it should be published without  
his prior written consent and information derived  
from it should be acknowledged.

**July 1992**



**14 JAN 1994**

I certify, that neither my thesis nor the original work contained herein has been submitted to this or any other institution for a degree.

The Copyright of this thesis rests with the Author. No part of it may be published without prior written consent and any information derived from it should be Acknowledged.

**Acknowledgements:**

I would like to thank Dr T.V.Parry for his valuable advice and patience as I went through many changes at ICI.

I would also like to extend my heart felt gratitude to Dr I.M.Robinson for his tireless advice throughout and particularly at writing up time, and also for arranging for me to use the Raman apparatus at Queen Mary WestField college, London.

Many thanks also to Dr Costas Galiotis and his staff for allowing me to use the Raman apparatus and his professional advice.

Many thanks to Dr Roy (Cliche King) Moore for his financial assistance.

And Finally I would like to thank my wife Jill, for badgering me to finish on time, without her intervention I would still be sitting on the data.

## 1 List of Figures

- Fig 1 Interface modulus effect on a) Composite strength b) Composite Modulus.
- Fig 2 Interfacial shear stress patterns for the elastic matrix case.
- Fig 3 Fibre pull out test.
- Fig 4 Critical embedment length.
- Fig 5 Single filament shear energy test.
- Fig 6 Specimen for measuring the debond energy of fibre.
- Fig 7 Specimen for measuring interfacial shear.
- Fig 8 Specimen for measuring interfacial tranverse tensile strength.
- Fig 9 Fibre fracture and stress distribution.
- Fig 10 Scattering of unpolarised electromagnetic radiation.
- Fig 12 Schematic of Laser Raman apparatus.
- Fig 13a Peaks in PDA fibres.
- Fig 13b Measured peak in PDA fibres.
- Fig 14 P75/Nylon prior to heating.
- Fig 15 P75/Nylon after 120 seconds laser heating.
- Fig 16 Torsional modulus apparatus.

**Fig 17** Torsional modulus plots for long fibre/PA Live feed moulded samples.

**Fig 18** Torsional modulus plots for short fibre/PA Live feed moulded samples.

**Fig 19** Torsional modulus plots for long fibre/PA conventionally moulded samples.

**Fig 20** Torsional modulus plots for short fibre/PA conventionally moulded samples.

**Fig 21** Short glass fibre/PA tensile dilatometry fracture surfaces.

**Fig 22** Long glass fibre/PA tensile dilatometry fracture surfaces.

**Fig 23** Interface badly degraded by moisture uptake.

## TABLE OF CONTENTS

		PAGE NO
1	INTRODUCTION	1
2	THEORY OF FIBRE INTERFACE	3
2.1	The Fibre Matrix Interface	3
2.1.1	Adsorption Wetting and Interdiffusion	3
2.1.2	Chemical Bonding	5
2.1.3	Fibres and Fibre Assemblies	7
2.1.4	Glass Fibres	9
2.2	Role of the Interface in Composite Materials	12
2.3	Interface Properties with Respect to Composite Performance	15
2.4	Load Transfer Theories in Composites	21
2.4.1	Stress Transfer from Matrix to Fibre	21
2.5	Methods for Measuring Interfacial Bond Strength	30
2.5.1	Fibre Pull Out Test	30
2.5.2	Single Filament Shear Fracture Energy Test	39
2.5.3	Interfacial Shear Stress and Transverse Tensile Strength	43
2.5.4	Single Filament Critical Length Determination	46
2.6	Strain Measurements Using Optomechanics	49
2.6.1	Introduction to Optomechanics	50
2.6.2	Light scattering and the Raman Effect	51
2.6.3	Resonance Raman scattering	58

3	EXPERIMENTAL DETAILS	64
3.1	Materials Under Study	64
3.2	Strain Measurements in Single Fibre Composites	67
3.3	Reproductivity Trials	73
3.4	Single Fibre Tests	74
3.4.1	Critical Length Measurements for Certain PA/Fibre Systems	79
3.5	Fibre Length Distributions	80
4	TORSIONAL AND FLEXURAL STIFFNESS OF LONG/SHORT FIBRE NYLON COMPOSITES	92
5	DISCUSSION AND CONCLUSIONS	109
6	REFERENCES	111

## 1 Introduction

Fibre reinforced composites are not new materials, they occur naturally i.e wood which is composed primarily of cellulose chains embedded in a lignin matrix . One of the earliest man-made composites may have been building blocks made with straw as the reinforcing fibre dispersed in mud as the matrix.

This report will deal with the properties high performance fibre composites made with high strength filaments such as glass and carbon fibres dispersed in a thermo-plastic matrix, with special emphasis on the interface between the fibre and matrix .

Fibre composites are a growing class of materials with high strength and modulus and low density . Modulus and strength values for carbon composites in the fibre direction are in the same order of magnitude as for high strength steel but



with a relative density of only one fifth. Weight for weight the composite strength is some five times larger than steel. Such composites are finding increasing usage in the aerospace, shipbuilding, recreational equipment and to an increasing degree in automobile parts [1,2,3].

Composite manufacturers exploit the stiffness and strength of high performance fibres by dispersing them in a resin matrix which acts as a binder and transfers force from one fibre to another. However the interfacial region between fibres and matrix is critical and governs the transfers the forces between the relatively weak matrix and the reinforcing fibres. An interface is specific for the particular fibre-matrix system used, however there are generalities that apply to all systems.

## **2 Theory of fibre/matrix interface**

### **2.1 The fibre/matrix interface**

The adhesion of a fibre to the matrix at the interface can be attributed to the following mechanisms according to Hull [4].

#### **2.1.1 Adsorption wetting and interdiffusion.**

The most important factor during the manufacture of a composite is the wetting of the fibres by the polymer matrix. For efficient wetting to occur the surface energy of the fibre must be greater than that of the polymer used. For example Glass and Graphite fibres with surface energies of 560 and 70 MJm<sup>-2</sup> respectively calculated by Kelly [5], should be easily wetted by Polyester and Epoxy resins with respective surface energies of 35 and 43 MJm<sup>-2</sup>. On the other hand Polyethylene fibres with surface

a energy of  $31 \text{ MJm}^{-2}$  require surface treatment in order to be wetted by these same resins. This points to the fact that although surface energy is important, if at any stage a chemical reaction occurs between the fibres and matrix either naturally or by thermal persuasion, then the initial surface energies may not be a dominant factor in the strength of final bond achieved between fibre and resin matrix.

A bond between two surfaces may be formed by the diffusion of molecules of one surface to the other. The strength of which is dependent on the level of molecular entanglement, the number of molecules present and the strength of the intermolecular bond.

### 2.1.2 Chemical bonding

Another important factor for bonding to occur between fibre and matrix is the chemical reaction at the fibre/matrix interface. Increased chemical bonding can be achieved by a variety of methods. In the case of a glass fibre/epoxy resin composite bonding is enhanced by first coating the fibres with silane. The bonding is explained by a chemical reaction between the silane and fibre and fibre surface and silane and matrix. With carbon fibres chemical bonding is promoted by oxidising the fibre surface, this bonding can also be explained by chemical bond between the surface of the oxidised carbon fibre and the resin matrix. Considerable effort has been put into determining the effect of pretreating and adhesion of thermo-plastic fibre composites. Kodikian [6] suggested that chemical modification of the surface of the thermo-plastic by the introduction of specific groups

will increase the degree of interfacial contact and intrinsic adhesion. The composites referred to are APC-2 ( ICI CF/PEEK ) and 913c XAS-5-34% ( Ciba- Geigy). A range of surface treatments were carried out and tested using the double cantilever beam (DCB) geometry [7] to measure the critical strain energy release rate  $G_{IC}$ . Results suggest for APC-2 the presence of a weak boundary layer which may in part be due to the release agents used. A possible cause for the interfacial failure could also be poor wettability and intrinsic adhesion of the thermo-plastic surface relative to epoxy adhesives. Corona discharge pretreatment was employed since it is known to frequently increase the wettability of poor bonding substrate's. Initial results show that Corona treatment may lead to increase in the  $G_{IC}$  for the thermo-plastic APC-2 composite bonded with epoxy based adhesives.

### 2.1.3 Fibres and fibre assemblies

Surprisingly carbon fibres were firstly developed and commercially used over a century ago by Swan and Edison in the first electric light bulbs. They carbonised viscose rayon or cotton to make their incandescent filaments, but the material was replaced with tungsten. An alternative route to carbon fibre used PAN continuous twine. PAN is a polymer closely resembling polyethylene in molecular conformation in which every alternate hydrogen side group of the polyethylene is replaced by a nitrile( $\text{-C}\backslash\backslash\text{N}$ ) grouping. The reason why PAN is used is that the nitrile side groups in can react together to form a ladder like polymeric structure.

The process can be split in to 4 four simplified steps;

- a) Hot stretch orientation of PAN twine (~400K)
- b) Formation of ladder polymer (~600K)

c) Chain oxidation followed by pyrolysis (~1300K)

d) Pyrolysis and carbonation (~2300K) to produce graphitic sheets.

All these processes are amenable to further development and increased sophistication. There are advantages and disadvantages attached according to performance, cost and ease of manufacture and quality of final product.

#### **2.1.4 Glass Fibres**

There are several types of glass fibre available, which are designated different letter codes.

E-Glass commonly used in the production of Vertron and Plytron (ICI- Advanced Materials), is a borosilicate glass very similar in composition to Pyrex. It was developed for electrical uses and has good resistance to water and acids.

C-Glass is a chemically resistant grade which withstands acidic, alkaline and aqueous environments.

S-Glass is an Aluminium-Magnesium silicate glass of higher strength and modulus and consequently more expensive.

Glass fibres are made by drawing them in parallel from the melt through platinum dies. The fibre diameter is determined by a careful balance between viscosity, surface tension of the molten glass, die diameter and haul off speed. Fibres are then coated with a size to protect

them from abrasion upon contact with one another.

Fibre type	Density $Kgm^{-3}$	Modulus $GNm^{-2}$
Aramid Kevlar 29	1400	60
Aramid Kevlar 49	1440	124
Carbon Fibre HM	1850	480
Carbon Fibre HS	1760	265
Pitch Fibres P75		570
Nylon 6 Perlon	1130	0.7
Nylon 6,6	1140	1.0
PET Dacron/Terylene	1400	12.3
E-Glass	2550	72
S-Glass	2490	87

**Table 1: Modulus and density of commonly used fibres**

## **2.2 Role of the interface in composite materials**

Of the many factors that govern the characteristics of a fibrous composite the level of adhesion at the fibre/matrix interface plays an important role in the structural properties of two phase materials. There are a numerous methods by which interfacial adhesion can be studied both directly and indirectly. The most commonly utilised techniques will be discussed. In interfacial failure mode studies, two extreme cases occur in tension for a weak interface can be identified. Fibre pull out [8] is responsible for rupture and is due to the fact that the fibres are not bonded by the matrix and are free to slide in their matrix cavities and it is not possible for load to be transferred to the fibres in such a discontinuous medium. The composite fails in a shear mode usually at a low applied stress. In the case of strong interfacial bonds load is transferred from matrix to fibre until it

reaches the breaking strength of the fibres. This leads to sudden and catastrophic failure, a higher interfacial shear is associated with this kind of failure.

All commercial fibres are surface treated to increase their wettability, since virgin carbon fibres exhibit low bondability to all polymer matrices. These surface treatments are oxidative which introduce functional groups on the fibre surface to enhance wettability. It must be pointed out that carbon fibre strength is flaw sensitive. Extensive oxidation and etching can increase surface flaws which leads to a reduction in tensile strength of the fibres.

Studies to optimise functional groups on the fibre surface and reduce possible effects of excessive oxidation/etching have been conducted by many workers, for example Ehrburger [9], Molleyre and Bostick [10], Fitzer et al [11]. Goan et

al [12] investigated the sodium chlorate/sulphuric acid oxidation process. This doubled the short beam shear strength , but also lead to a 5% reduction in tensile strength. In certain applications this sacrifice may prove to be a worthwhile.

Ehburger & Donnet [13] and Pinchin & Woodhams [14] discovered that by insertion of a weak acid group the short beam shear strength could be enhanced as much as with strong acid groups. The mode of failure differs, with strong acid groups tensile failure was observed. A plausible explanation for this could be that weak acidic groups increase the surface energetics of fibres which in turn gave better wetting and adsorption which improves the coupling. The strong Carboxylic and Phenolic acid groups couple to the matrix through tighter and stronger primary bonds at the interface which creates a brittle composite.

### **2.3 Interface properties with respect to composite performance**

General commercially available carbon fibres are usually sized with an epoxy compatible size to improve handling capabilities and also act as lubricants and as a " loose binder" to prevent fibre fuzz and to enhance interfacial bonding.

Size materials are often applied in a very thin layer, approximately 1.5% by weight of the fibre, this is equivalent to a coating of 800A thick.

Due to the small size of the interphase very few analytical techniques can be applied. Further more the fibre geometry and low atomic number elements on the surface add to the difficulties in understanding the interphase in composites. Several workers have observed effects of the interphase indirectly by using mechanical tests.

Pinchin and Woodhans [14] increased the fibre surface energetics by pyrolysing graphite onto the carbon surface. An increase in shear and flexural strength was observed as well as a small improvement in impact toughness. A feasible hypothesis for this could be that the pyrolytic graphite deposit forms a sheath around the fibre which itself creates an additional interface and during any crack propagation/debonding process. This new interface absorbs more energy by exposing additional free surfaces.

Broutmann and Agarwal [15, 16] carried out a theoretical study on an interphase layer. They assumed both phases behaved elastically and have perfect bonding at the interface. It was observed that composite strength reached a maximum when the interface modulus reached a value of 69 MPa (Figure 1). It must be noted that Broutmann referred to interface modulus but by definition the interface is deemed to have zero thickness so the term interphase appears more appropriate. However, experimental data does not

support Broutmann's theory and the critical interphase modulus determined in his study is considerably lower than the matrix modulus. This approach is similar to the flexible interlayer concept by Di-Benedetto and Nicolais [17]. Since there is a difference in thermal expansion co-efficient of fibre and matrix, elevated temperature curing will accumulate residual stress at the interface. This interfacial stress is increased further due to matrix shrinkage during polymerisation and by incorporating a flexible interlayer residual stresses can be relieved.

Lavengood [18] coated boron and glass fibres with a low cross linking epoxy system to form a thick flexible interlayer. An increase in mechanical properties of both moisture conditioned and unconditioned samples was observed. A 1000 fold increase in torsional fatigue life was recorded (Figure 2) shows the improvement in transverse properties of glass fibre /epoxy composites by incorporating a soft interphase. In addition to mechanical properties

of the interphase its thickness is critical in order to optimise composite properties. When a silicone rubber exceeds 1% by weight Hancox and Wells [19] observed a considerable decrease in flexural strength.

A novel approach was used by Atkins [20] where bonding along the fibre surface was intermittent, the weakly bonded regions would allow debonding and fibre pull out during fracture whilst load transfer was achieved by the strongly bonded sections. Such a combination provides high fracture toughness and good tensile strength.

Reiss et al [21] suggested a two phase block co-polymer, polyisoprene-polystyrene-maleic anhydride at the interface. While the polyisoprene provides the energy absorbing capabilities and the styrene-maleic anhydride enhances the compatibility and joint strength of the fibre with the matrix. Increased shear strength in both moisture conditioned and unconditioned was measured along with an increase in fracture toughness.

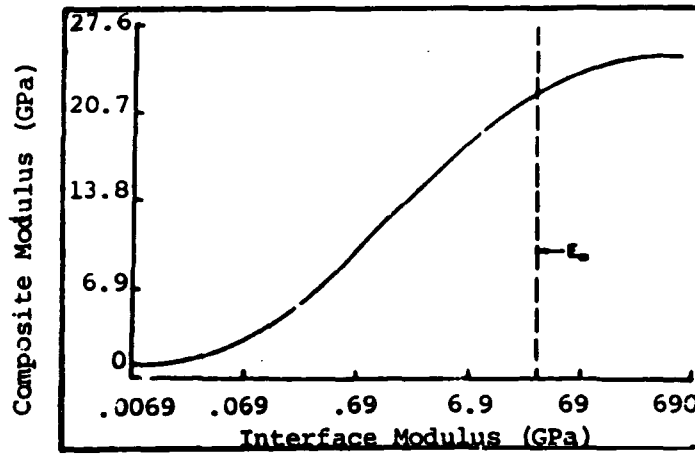
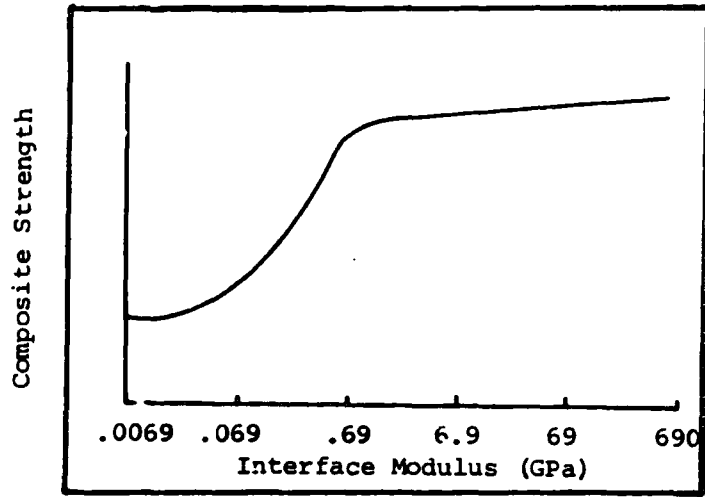


Figure 1

Interface (interphase) modulus effect on  
 (a) Composite strength  
 (b) Composite modulus

All previously discussed work on interface/interphase indicates that composite toughness can be increased without the accompanying degradation of the remaining mechanical properties by proper selection of the interphase properties such as glass transition temperature ( $T_g$ ), modulus ( $E$ ), strength ( $\sigma$ ) etc. and its physical characteristics such as thickness.

## **2.4 Load transfer theories in composites**

### **2.4.1 Stress transfer from matrix to fibre**

If a load is applied to an elastic matrix, the matrix will elongate to a value proportional to the load. Furthermore, if a fibre with a higher elastic modulus is embedded into this matrix, the fibre will restrict the elongation of the matrix in the fibre direction. Shear stresses are produced parallel to the fibre axis in the direction of this axis. These shear stresses in turn induce tensile stresses in the fibre. Birefringence techniques have been used to evaluate these stress patterns.

Several models are available for calculating longitudinal tensile stress distribution in an embedded fibre. Rosen, Cox and Dow [21, 22, 23] considered the case of an elastic fibre in an elastic matrix and derived expressions for direct tensile stress in the fibre and for interfacial

shear stress along the interface, for any given stress applied to the matrix. The tensile strain of matrix and fibre are nearly equal at the mid length. When a load is applied to the fibre by shear stress at the interface physically, at equilibrium.

$$\frac{dP}{dx} = \pi d_f \tau_x \dots (1)$$

when  $x$  = distance from end of hole

$d_f$  = diameter of fibre

$P$  = tensile load in the fibre

$\tau_x$  = the stress evaluated at the fibre surface.

The magnitude of the shear stress is dependent on several factors such as, the fibre content, the magnitude of the load applied and on the physical properties of the filament, matrix and interfacial bonds.

Several assumptions are made in order to obtain an expression for shear stress.

1 Fibre and matrix behave elastically

2 The fibre is surrounded by a cylinder of matrix material

3 The bond between fibre and matrix is perfect throughout any deformation.

4 Straight radial lines in the fibre and matrix remain straight lines after deformation.

5) Stress distribution around one fibre does not influence

that around another.

The shear stress between fibre and matrix can be expressed as follows;

$$\frac{\lambda}{4} \left( \frac{P_{eff}}{(A_m E_f)} + \alpha_f \right) * \left( \frac{\left( \sinh \frac{\lambda}{d_f} \left( \frac{l}{2} - x \right) \right)}{\left( \cosh \frac{\lambda}{2} * \frac{l}{d_f} \right)} \right) \dots\dots\dots 1$$

$$0 < x < l/2$$

where

$$\lambda = 2 \left( 2 * \frac{\left( 2 \frac{G_f}{E} * 1 + \frac{A_f}{A_m} * \left( \frac{E_f}{E_m} \right) \right)}{\left( 2 - l + \left( \frac{G_f}{G_m} \right) * \left( \frac{A_m}{A_f} + 2 \right) \right)} \right) \dots\dots\dots 2$$

and

$\tau_x$  = Interfacial shear stress

$E$  = Youngs modulus

$A$  = cross sectional area

$G$  =shear modulus

$x$  =distance from end of fibre

$l$  =effective length for load differential between fibre  
and matrix

$d_f$  =diameter of fibre

$$P_{eff} = 8\sigma A_m \left( 1 - \frac{E_m}{E_f} \right)$$

$\sigma_a$  = *applied field stress (MPa)*

subscripts f and m refer to fibre and matrix, respectively.

The tensile load in the fibre at  $x$  is calculated thus ;

$$x = \pi d_f \int_0^x \tau_x dx$$

by integrating the above equation the tensile stress in  
a fibre at position  $x$  can be found

$$\sigma_f = \delta_a k \left( 1 - \frac{\cosh \frac{\lambda}{d_f} \left( \frac{l}{2} - x \right)}{\cosh \left( \frac{\lambda l}{2} d_f \right)} \right) \dots\dots\dots 3$$

where

$$k = 1 + \left( \frac{1 - \frac{E_m}{E_f}}{\frac{E_m}{E_f} + \frac{A_f}{A_m}} \right)$$

The transfer length required to build up a maximum stress equal to  $\phi$  of the stress in an infinitely long fibre can also be calculated from the following equation;

$$\frac{l_c}{d_f} = \left( \frac{l}{\lambda} \cosh^{-1} \frac{l}{l - \phi} \right) \dots\dots\dots 4$$

the load transfer pattern is shown in figure 2.

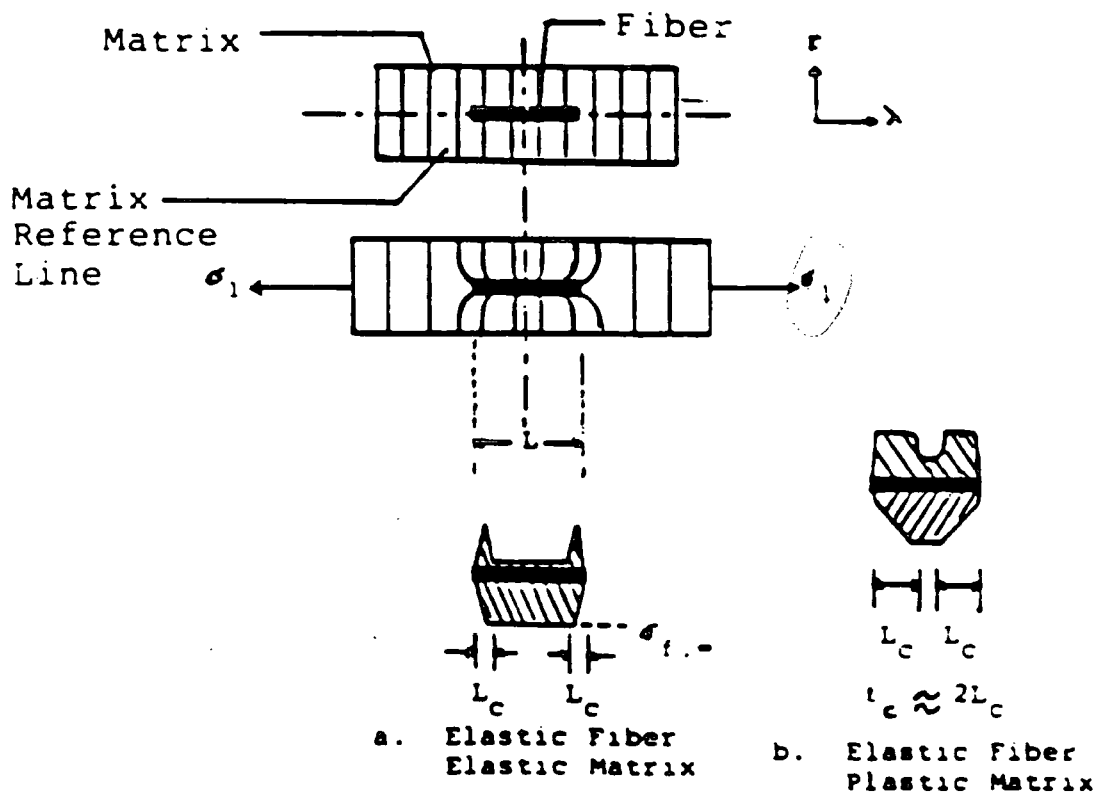


Fig 2 Interfacial shear stress patterns for the elastic matrix case

From equation 1 it is clear that maximum shear occurs at the ends of the fibre. When a tensile load is applied the shear stress is likely to exceed the yield stress of the matrix. If the matrix is unable to plastically deform, either the matrix fails or an interfacial slip occurs between the fibre and matrix. However if the matrix is able to deform then the interfacial shear stress never rises above the yield strength of the matrix and equation 1 becomes irrelevant, therefore the plastic flow model of Kelly and Tyson [5] is more appropriate. For a perfectly plastic material, yield strength remains constant throughout the deformation. A tensile stress distribution in the fibre can be obtained by integrating ;

$$P = \sigma_f A_f = \int_0^x \pi d_f \tau_y dx \dots \dots \dots 5$$

$$= \pi d_f \tau_y x$$

the tensile load builds up linearly and a transfer length of the fibre is obtained.

$$\frac{l_c}{d_f} = \frac{\sigma_f}{4\tau_y} \dots\dots\dots 6$$

Or

$$\lambda_y = \frac{\sigma_f d_f}{2l_c} \dots\dots\dots 7$$

$\sigma_f$  = tensile stress of fibre at transfer length

$d_f$  = fibre diameter

$\tau_y$  = interfacial shear strength

$l_c$  = critical fibre length required for load transfer

## **2.5 Methods for measuring interfacial bond strength**

There are several tests which are commonly used for measuring interfacial bond strength. Some methods , such as the critical fibre length technique offer promise with more in depth research. The critical length technique and other techniques will be considered in greater detail.

### **2.5.1 Fibre pull out test**

The single fibre pull out test was developed by Broutmann [24] to measure the interfacial joint strength and interfacial functional strength. Two different geometries are currently available for the pull out test, they can be of a button type (Figure 3) or a calculated length of fibre length embedded into the bulk matrix .

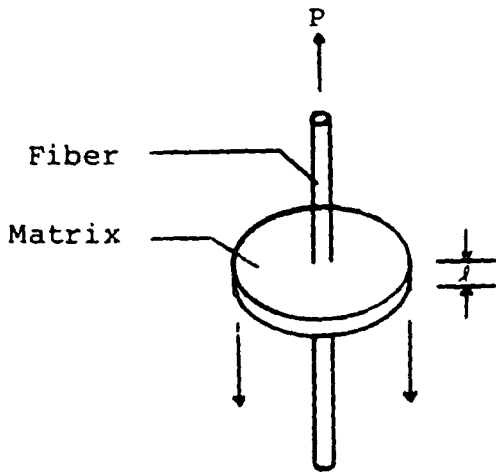


Fig 3 Button type specimen for fibre pull-out test.

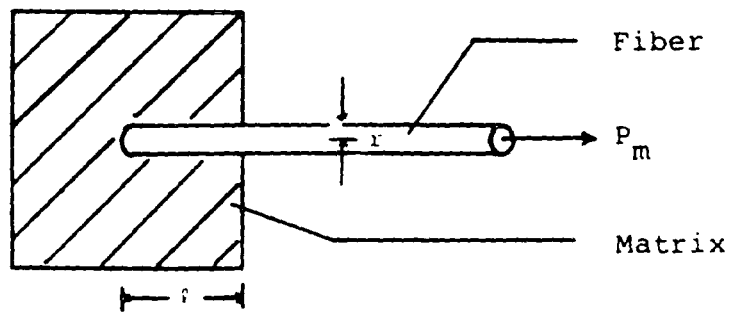


Fig 3b Block type specimen for fibre pull-out test.

The relationship below assumes the shear stress to be uniformly distributed along the interface.

$$\tau = \frac{P_m}{2\pi r l} = \frac{\sigma_m r}{2l} \dots\dots\dots 8$$

Where

$\tau$  = average shear strength of joint

$P_m$  = maximum load applied to the fibre

$r$  = radius of fibre

$l$  = embedded length of fibre

$\sigma_m$  = maximum strength applied to fibre

The maximum embedded length is dependent on fibre strength and is determined by;

$$l_{\max} = \frac{\sigma_{ult} r}{2\tau}$$

$\sigma_{ult}$  = ultimate tensile strength of fibre

Lawrence P and Bartos P [25, 26] carried out a theoretical analysis of this test and concluded that it was sensitive to interfacial adhesion properties. The application of this test to carbon fibre/epoxy systems is problematic due to the small diameter of the fibre and relatively high interfacial bond strength. Typically the maximum embedded length of fibre of such a system must be less than 0.1 mm.

A relatively simple method for determining the critical embedment length would be to test several single fibre specimens with various embedment length and equating the fibre pull out force to the embedded length (Figure 4).

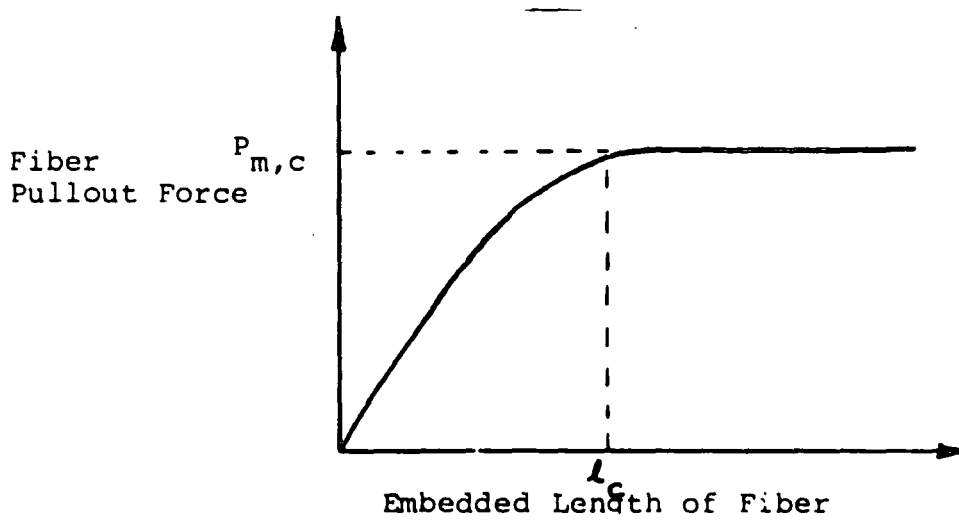


Fig 4 Critical embedded length.

According to Lawrence and Bartos [25, 26] the joint strength must be calculated using;

$$\tau = \frac{P_{mc}}{\pi d l_c}$$

$P_{mc}$  = maximum pull out force at maximum embedded length

$l_c$  = maximum pull out length which allows fibre pull out

there is difficulty in verifying the above theory due to problems fabricating ultra thin lozenges.

The basic assumptions of shear lag theory are that all the loads are carried by the matrix and the load transfer into the fibre occurs from the matrix over a length of fibre called the ineffective length  $l$ . If the shear strength of fibre whose embedded length is greater than the ineffective length is calculated using equation 1, then the shear stress will be under estimated. This is because a length of fibre is included over which no stress

transfer occurs so, the smaller the embedded length the greater the estimate of the shear strength. In theory, the maximum shear strength should be obtained when the embedded length tends towards zero.

Grezczuk [27] has applied the shear lag equation to a single fibre, one end of which is embedded in a resin

$$\tau_{\max} = \tau_{av} a l \coth a l$$

$\tau_{av}$  = average intrerfacial shear strength

$l$  = embedded fibre length

$a$  = constant given by  $a = \left( \frac{2G}{brE_f} \right) \dots \dots \dots 3$

where

$G$  = interfacial shear modulus

$b$  = interface thickness

$r$  = fibre radius

$E_f$  = fibre modulus

No accurate means of calculating G and b exist at present. Pitkethly and Doble [28] have derived a procedure by which "a" can be eliminated and a single value is established for  $\tau_{\max}$ .

The final expression obtained is :

$$\operatorname{arctanh}\left(\frac{\tau_{av} L}{m}\right) = \tau_{\max} \frac{L}{m}$$

a plot of  $\left(\tau_{av} \frac{L}{m}\right) v \left(\frac{L}{m}\right)$

the slope of this curve will enable us to calculate  $\tau_{\max}$

The parameters required using this technique are the fibre diameter, the embedded length and the pull out force.  $\tau_{av}$  is calculated using equation 1.  $\tau_{av}$  &  $L$  are used to calculate the interfacial shear strength as above. This method gives good agreement between theory and experiment.

Additionally, this method gives information regarding the interface shear modulus  $G$  and the interface thickness  $b$  which is fundamental to the micro mechanical modelling of the interface region.

The only draw back seems to be the understanding of the failure mechanisms. Penn and Lee [29] have attempted to explain this using a fracture mechanics approach. They also conclude that the relationship between  $P_m$  ( pull out force and initial embedded length) is not linear but exhibits a dual behaviour of rising force at low embedded lengths followed by constant force at higher lengths. This leads to the conclusion that there is no unique bond strength over all values of  $L$ .

### 2.5.2 Single filament shear fracture energy test

Murphy and Outwater [30, 31] developed a relatively simple test for measuring the debonding fracture energy between an epoxy resin and a glass fibre, it consists of a long fibre of diameter  $d_f$  and cross section  $A_f$  embedded in semi infinite resin (figure 5).

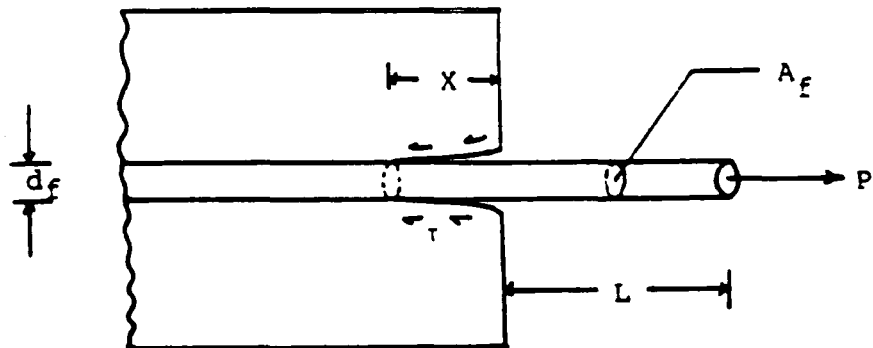


Fig 5 Single filament shear energy test specimen  
Murphy and Outwater.

If P is the tensile force at the end of the fibre and the fibre is debonded at a distance x into the matrix and  $G_{II}$  is the energy required to debond the fibre then ;

$$G_{II} \frac{8E_f}{d_f} = \left( \sigma - 4\tau \frac{x}{d_f} \right)$$

$\tau$ =interfacial strength

$E_f$ =modulus of fibre

$\sigma$ =stress at free end

The obvious difficulty with this set up is that the fibre must be directly pulled which makes it experimentally tricky. This technique was modified so the whole fibre is embedded in a resin block and the fibre is severed at the centre. The specimen is then loaded in compression and load is observed until the fibre debonds (Figure 6).

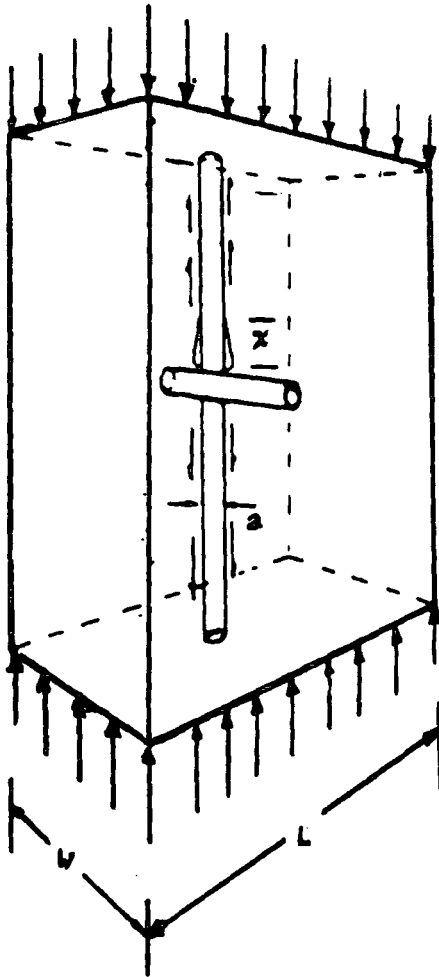


Fig 6 Specimen for measuring the debonding energy of the fibre from surrounding matrix.

calculate  $G_{II}$

$$G_{II} = \sigma_r \left( \frac{E_f}{E_r} \right) - \left( 4\tau \frac{x}{d_f} \right) \left( \frac{d_f}{8E_f} \right)$$

where;

$\sigma_r$  = applied stress

$x$  = bond length

$E_r$  = compressive stress of resin

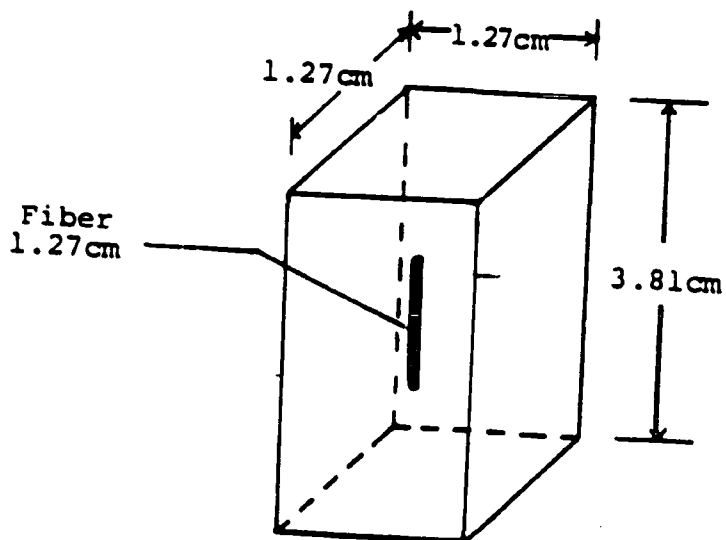
for initiation  $x=0$

$$G_{II} = E_r^2 E_f d_f \text{ over } 8$$

This test is suitable for glass fibres in an epoxy matrix, however due to the relatively small diameter and brittle nature of carbon fibres this test would not be applicable for carbon fibre/epoxy systems. The initial debonding during compression may be observed using a portable microscope.

### 2.5.3 Interfacial shear stress and transverse tensile strength

Broutmann also developed a test for the characterisation of interfacial shear debonding strength and interfacial transverse tensile strength. This is accomplished by embedding a single fibre filament in the centre of an epoxy casting (Figure 7)



$$\tau = 2.5\sigma$$

Figure 7 Interfacial shear debond strength specimen.

$$\tau = 2.5\sigma$$

where

$\sigma$  =axial compressive stress of specimen

The interfacial transverse tensile strength is determined using specimens with a curved matrix (Figure 8).

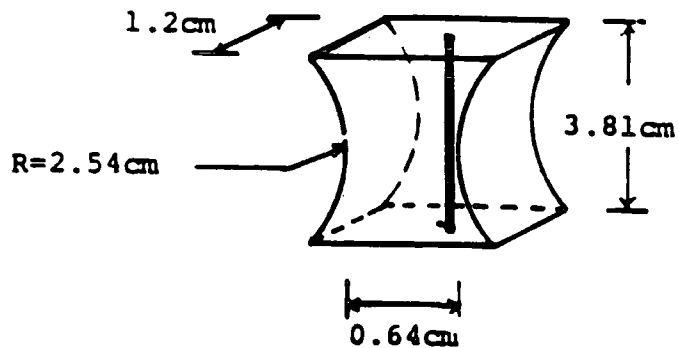


Figure 8. Interfacial transverse tensile strength specimen.

Debonding at the interface will occur via transverse tensile stress due to the difference in Poisson's ratio of the fibre and matrix and of course due to curvature of matrix.

The transverse tensile stress is calculated by;

$$S = \frac{\sigma_m(\mu_m - \mu_f) E_f}{(1 + \mu_m) E_f + (1 - \mu_f - 2\mu_f^2) E_m}$$

where

$S$  = transverse tensile stress

$\mu$  = Poisson's ratio

$E$  = elastic modulus

Several workers have used this experiment for evaluating adhesion properties. However, this test is unsuitable as it relies on fibres having high compressive failure strain and, during testing, matrix cracking and/or fibre buckling may occur before debonding of the fibre.

#### 2.5.4 Single filament critical length determination

Kelly [32] illustrated the multiple fracture phenomenon using a model system consisting of tungsten wires embedded in a copper matrix. After deformation, the copper matrix was dissolved away and the wire fragments extracted. Upon close examination of the fibre fragments, the length distribution was found to have bounds

$$l_c > \frac{l_c}{2}$$

Where the critical fibre length was determined from;

$$l_c = \frac{\sigma_f d_f}{2\tau_y}$$

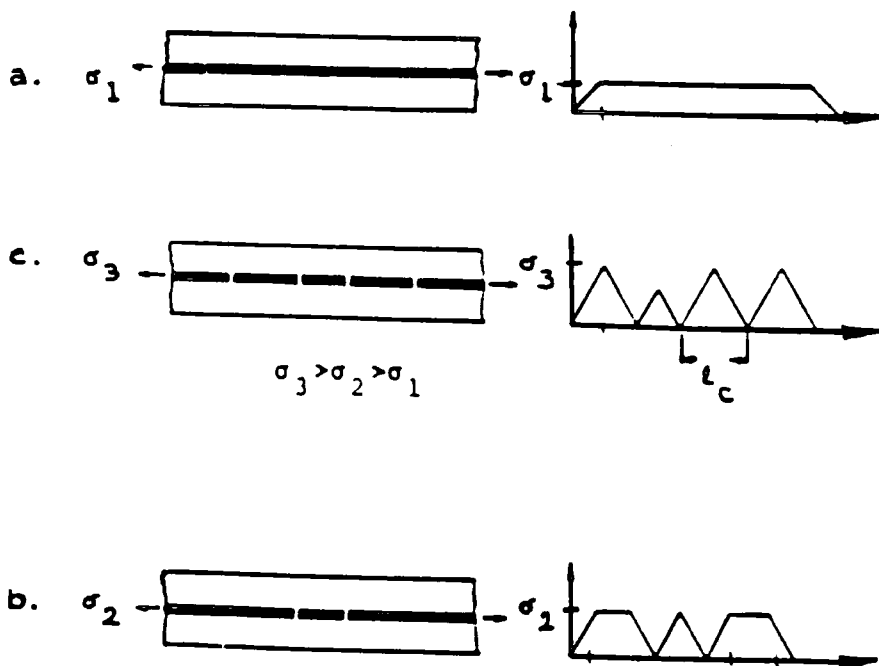
where

$\sigma_f$  = tensile strength of fibre

$d_f$  = diameter of fibre

$\tau_y$  = interfacial shear strength

Parallel experiments were run by McGarry & Fujiwara [33], Frazer et al [34], Onigchin et al [35] using glass fibres in thermosetting and thermo-plastic matrices, the results proved to be inconclusive. Ishikawa et al [36] applied this technique to carbon fibres in an epoxy matrix. The critical length distribution is shown in (Figure 9)



Fibre fracture and stress distribution.

Figure 9 Critical length distribution plots.

Drzal et al [37], Di-Benedetto & Nicolais [38] and McMahon & Ying [39] proposed similar expressions but all the authors have assumed a constant shear at the interface, but choose to ignore the matrix properties a condition which cannot seriously be met in a real fibre reinforced composite. The practice of measuring the interfacial shear strength from experimental  $l_c$  values rather than calculating it from the matrix yield strength as originally proposed is questionable.

## **2.6 Strain measurements using Optomechanics**

### **2.6.1 Introduction to optomechanics**

Experimental techniques which fit under this category are birefringent coatings, photoelasticity, holography and Moire methods. These techniques give an indirect measure of the state of stress and strain for particular models representing the structure of interest. The stress field in a two dimensional slice of a stressed body made from a birefringent material can be determined by photoelasticity. Special variants of this technique can also measure a three dimensional stress field inside a birefringent material. The techniques are usually restricted to measuring surface stress strain fields.

Raman Spectroscopy can be used to measure directly the mechanical deformation inside certain polymeric materials. This is based on the fact that highly oriented polymers display vibrational spectra which are

stress-dependent. This is due to anharmonic bonding between the atoms along the polymer chain. Upon the application of a load the bonding in the polymer chain alters slightly resulting in a change in frequency change for the vibrational modes of the polymer which can be detected using vibrational spectroscopy.

Raman spectroscopy has been used to measure the point to point variation in strain in single glass and carbon fibres, both free standing and embedded in a Nylon matrix ( forming idealised single fibre composites ). The Raman method of measuring strain directly in oriented polymer composites forms the main optomechanical technique used in this study.

### **2.6.2 Light scattering and the Raman effect.**

Consider a molecule to be a spherical, polarizable electron cloud (Figure 10). If an electromagnetic wave of frequency  $\nu$  interacts with this cloud, it can cause it to oscillate at the same frequency. The extent to which this will occur will depend upon the polarizability or deformability of the electron. An oscillating electron cloud radiates in all directions. This radiation is called light scattering.

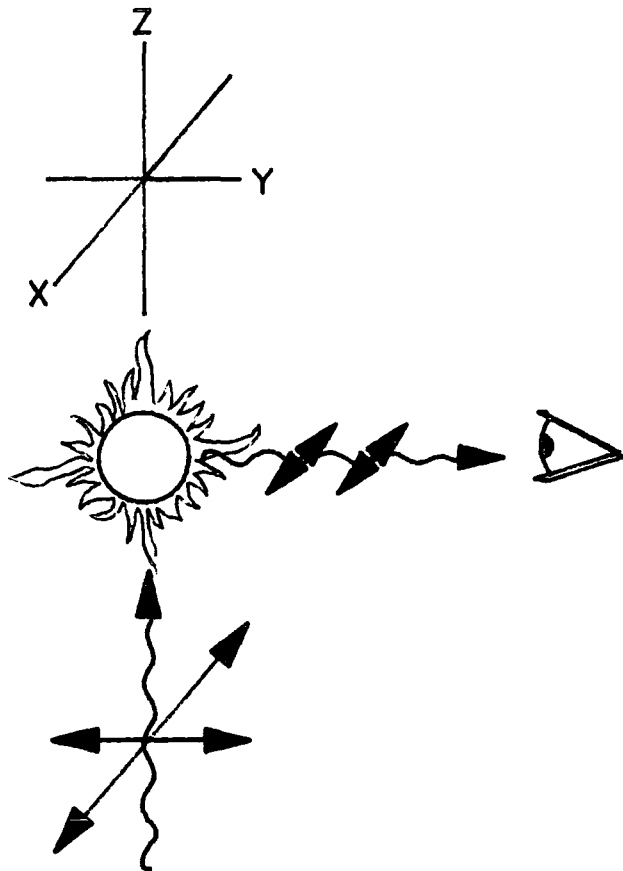


figure 10

Scattering of unpolarised electromagnetic radiation, incident along the Z direction, observed along the Y direction. For a spherical scatter, polarised scattered radiation is observed.

Suppose that the incident beam is along the  $z$  axis, and is unpolarised as shown in figure 10. The incident beam has electric vectors along  $x$  and  $y$ , and so the electron cloud will oscillate in the  $xy$  plane, since it is not possible to observe an electric field in the direction of propagation. The observer along  $y$  would observe polarised  $E_x$  radiation resulting from the scattering of unpolarised light incident along  $z$ .

In the Raman effect, the incident beam couples to molecular vibrations to give inelastic scattering, that is, the scattered radiation is of a different energy from the incident beam. If the molecule is approximately spherical to begin with (for example  $CH_4$ ) and the vibration is totally symmetric, then the polarisation is maintained as before. However if the vibration distorts the spherical symmetry, or if such symmetry does not exist to begin with, there may be significant intensity along the  $z$  direction in the observation along  $y$ . It suffices to

summarize by saying that for  $E_x$  polarized incident radiation (as is the general case for a modern laser source), incident along  $z$ , and analysis of the  $90^\circ$  scattered radiation along  $y$ , the depolarization ratio

$$p = \frac{I_z}{I_y}$$

ranges from 0 to 0.75. The range of values  $0 < P < 0.75$  is obtained for vibrational modes belonging to the totally symmetric representation, while all other modes, referred to as depolarised, yield  $P = 0.75$

The Raman effect can be predicted by classical arguments. The electric field  $E$  associated with an incident beam of frequency  $\nu_0$  can be written in its time dependent form as;

$$E = E_0 \cos 2\pi \nu_0 t$$

$E_0$  is the amplitude of the wave.

When this oscillating field interacts with the polarizable electric field, it induces a dipole

$$M = \alpha E$$

where  $\alpha$  is the polarisability of the material.

The Raman effect results from the interaction of the polarizability with normal modes ( $Q$ ) of vibration of the molecules. For the  $k$ th normal mode, it can be written as;

$$\alpha = \alpha^0 + \frac{\delta\alpha}{\delta Q_k} Q_k + \dots (\text{higher order terms})$$

$\alpha^0$

is the polarizability for the molecule with fixed nuclear positions.

The normal modes must be written in their time dependent form as

$$Q_k = Q_k^0 \cos 2\pi \nu_k t$$

substituting back into the expression for the induced dipole, thus

$$M = \alpha^0 E_0 \cos 2\pi \nu_0 t + E_0 \left( \frac{\delta \alpha}{\delta Q_k} \right) Q_k^0 (\cos 2\pi (\nu_0 + \nu_k) t + \cos 2\pi (\nu_0 - \nu_k) t)$$

The first term is the unshifted ( Rayleigh ) light scattering, while the second term gives the stokes and anti-stokes Raman frequencies of  $\nu_0 + \nu_k$ . This classical argument fails to predict the difference in intensity between these two combinations, a difference that results from the Boltzmann distribution of state populations.

In general, the induced moments should be written

$$M_x = \alpha_{xx} E_x + \alpha_{xy} E_y + \alpha_{xz} E_z$$

$$M_y = \alpha_{yx} E_x + \alpha_{yy} E_y + \alpha_{yz} E_z$$

$$M_z = \alpha_{zx} E_x + \alpha_{zy} E_y + \alpha_{zz} E_z$$

leading to an equation in the matrix form;

$$\begin{pmatrix} M_x \\ M_y \\ M_z \end{pmatrix} = \begin{pmatrix} E_x \\ E_y \\ E_z \end{pmatrix} \begin{pmatrix} \alpha_{xx} & \alpha_{xy} & \alpha_{xz} \\ \alpha_{yx} & \alpha_{yy} & \alpha_{yz} \\ \alpha_{zx} & \alpha_{zy} & \alpha_{zz} \end{pmatrix}$$

In actual practice, the intensities measured in an experiment will depend on the averages of the polarizability derivatives for an isotropic system such as a liquid or gas, or on a specific orientation for a system such as a single crystal.

### 2.6.3 Resonance Raman Scattering

Raman scattering is best explained by Robinson [40]. The intensity of Resonant Raman scattering is dependent upon the frequency of the incident radiation and for an initial vibrational level  $i$  given by;

$$I_f = N_i \frac{64\pi^2}{3C^2} (V_0 - V_{if})^4 P_{if}$$

where

$i$  = initial state

$f$  = final state

$N_i$  = population of molecules  $\epsilon$  the initial state

$P_{if}$  = electric moment associated with the transition from  $i$  to  $f$ .

this is related to the electric field vector of the existing radiation through;

$$P_{if} = \alpha_{if} E$$

With  $\alpha_{if}$  a property of the scattering molecule, it is

summed over all electronic states. As the excited radiation frequency tends towards that of an excited electronic state for the system, one sum dominates over all others. This is particularly the case in crystal structures, where selection rules remove certain components due to molecular symmetry. At this point we see a reduction in  $\alpha_{if}$

$$\alpha_{if} = \left(\frac{1}{h}\right) \left(\frac{\mu_{ef}\mu_{ie}}{V_{ie} - V_o}\right) + i\delta_e$$

where

$\delta_e$  = damping constant for excited state  $e$

$V_{ei}$  = frequency between ground state

$V_o$  = frequency of incident radiation

$\delta$  is related to the line width for a given state, a measure of the sharpness of an energy level. At room temperature only the ground and lower states are heavily populated. Vibrationally excited states can relax by fluorescent emission back to the ground state which is observed

experimentally as a broad fluorescent background. Strong resonant fluorescent times are seen for exciting frequencies greater than the frequency for an electronic transition.

#### 2.6.4 Tensile Dilatometry

For isotropic, homogenous materials the state of elasticity in the bulk can be described by four independent constants, Tensile modulus  $E$ , Shear modulus  $G$ , Bulk modulus  $K$ , and lateral contraction ratio  $\nu$ . These constants are related by a series of well established expressions, so if any two are known the other two may be calculated. As a consequence no one constant is more important than the other, though some are experimentally easier to determine than the others. In polymeric materials and their derivatives, these materials are inherently viscoelastic in nature and so are properly described as being pseudoelastic constants.

In the small deformation limit an applied stress may be analysed into tensorial components of the sum of the mean normal hydrostatic tensor and the deviatoric tensor. The hydrostatic stress results in a dilational response of the material i.e volume increase, while deviatoric (shear)

stress results in a change of shape with no change in volume. Any small deformation can be related to these two components of stress. However, in the large deformation limit, the hydrostatic tensile stress causing dilation may result in cavitation type mechanisms, producing a rapid increase in volume which leads eventually to fracture. The deviatoric stresses may result in shear yielding as the principal failure mechanism. In a material under large deformation one of these principle mechanisms will dominate the failure process. Consequently the characterisation of the dilational response of a material to an applied stress may lead to an appreciation of the deformation mechanisms present in the bulk of the material. The dilation response of a material to an applied stress can be understood in terms of the volumetric strain,  $v_s$ . This concept is best explained by Naqui and Robinson [42]. Experimental data for Long glass fibre/ Nylon composite and short glass fibre / Nylon composite using multiple

live feed mouldings and conventional mouldings at 23°C and 60°C in, dry and moisture conditioned state are presented.

Both the long and short fibre composites had a nominal fibre volume fraction of 40% in the skin and core regions.

### **3 Experimental Details**

#### **3.1 Materials under study**

The materials used in this study were as listed below;

1) Single fibres experiments,

a) P75, pitch based fibres.

2) Single fibre composite systems,

a) P75/Nylon

b) Glass/Nylon

3) Commercial Glass fibre filled composites

a) Long glass fibre/ Nylon conventional mouldings

b) Long glass fibre/ Nylon Multiple live feed injection  
mouldings

c) Short Glass fibre/ Nylon conventional injection moulding

d) Short Glass fibre/ Nylon multiple live feed injection moulding

The model composites were manufactured using a variety of techniques;

a) by sandwiching a single fibre between nylon film and then subjecting it to a combination of heat and pressure.

b) Placing a single fibre on top of the film and then gently running a soldering iron along the fibre, this causes the nylon to become tacky and the fibre embeds itself in to the matrix.

Great care was taken to ensure that the fibres were not damaged in any way and that the fibres were not kinked.

A range of specimens were manufactured e.g with continuous and discontinuous fibre's in the 0° direction, a few

specimens were also made using discontinuous fibre's in the 90° direction. Tensile specimens were cut out of the film with a die.

The multiple live feed short and long fibre composite plaques were supplied by Brunel university.

### 3.2 Strain Measurements in single fibre composites

The apparatus used are presented schematically in figure 12. Raman spectra were taken using an Argon ion green laser having a wave length of 514.53 nm. The laser power on all samples was always kept below 2 mW so as to avoid frequency shifts due to localised heating and to ensure no damage was caused to the specimen. A microscope was used to focus the incident laser beam onto a  $2\mu m$  spot on the fibre. The back scatter light was collected by the microscope objective using a  $100\mu m$  filter and double spectrograph monochromator . The detector was of the The intensified diode array type . Laser power was measured using a hand held power meter.

P75 fibres were subjected to tensile strain and the band shifts were recorded. For the PDA fibre at 0% strain three peaks were observed. These were located at

$2082cm^{-1}$

$1580cm^{-1}$

$1265\text{cm}^{-1}$

the 2082 line is associated with the stretching of the triple bond between carbon atoms Figure 13. The manufacturers quoted values of modulus and tensile strength were 510 GPa and 1.8 GPa respectively.

Since it is a known fact that Nylon fluoresces under laser light, several calibrations were made by focusing the laser

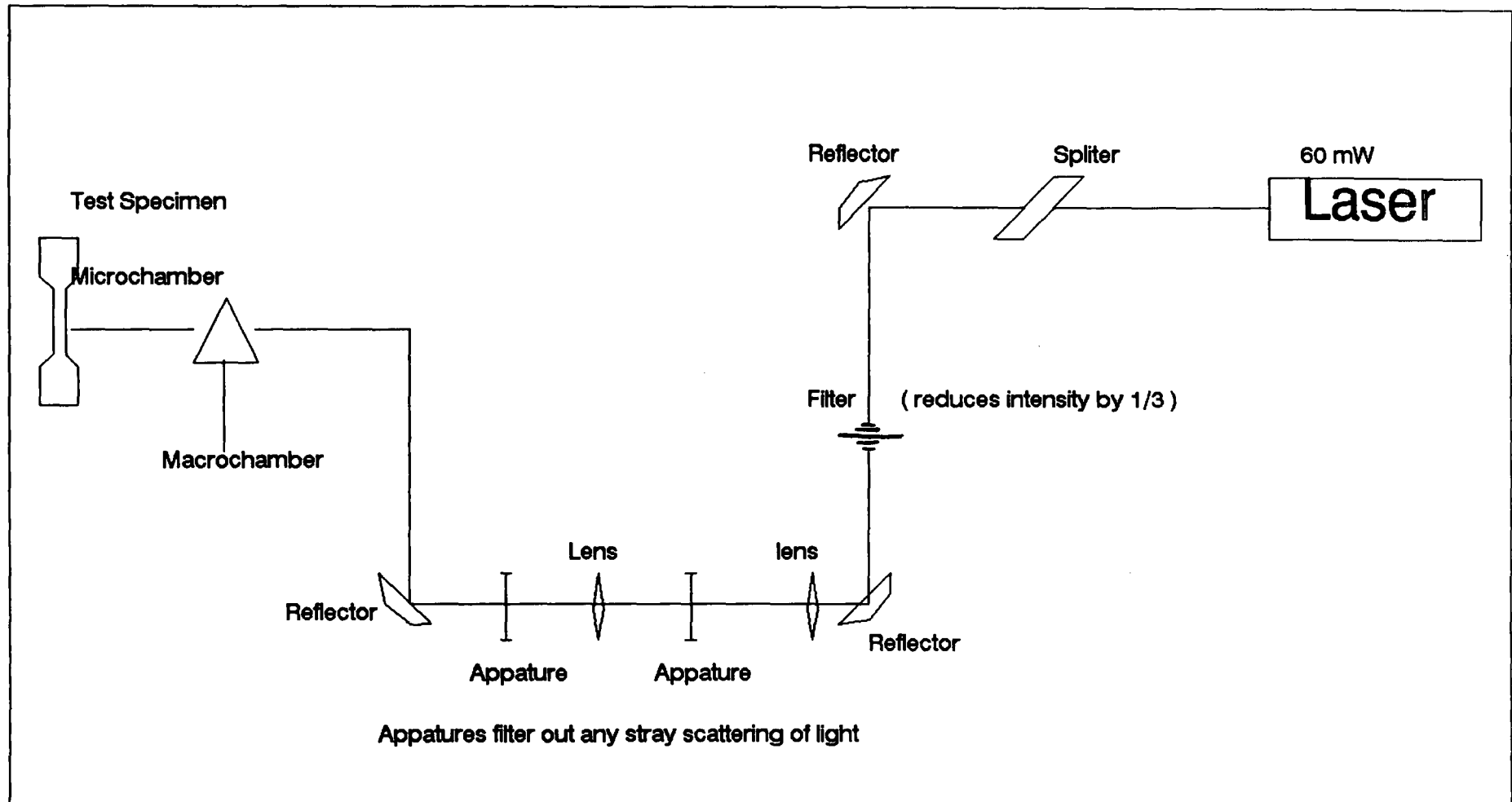


Figure 12

## Schematic set up of Laser Raman apparatus

on to Nylon film and the resulting data captured. The Nylon peak was observed at the  $1636\text{cm}^{-1}$  and  $2200\text{cm}^{-1}$ .

Polydiacetylene unit were used as a calibration check for the apparatus.

Once a strain is applied to the sample, minuscule stretching of the triple bond occurs, this leads to a change in the interatomic spacing which leads to a change in the electronic structure of the interatomic bonding. This is observed experimentally as a shift in the scattered Raman lines using an Argon laser focusing about 3mW onto the fibre. A peak was observed at  $2080\text{ cm}^{-1}$  for the poly diacetelyne fibre, see Fig 13b Consequently a band shift of  $-19\text{cm}^{-1}$  for PDA fibres and  $-9\text{cm}^{-1}$  for carbon fibres is observed. The area covered by the laser is approximately  $2\mu\text{m}$ . Several accumulations are carried out on each analysis point and each accumulation takes about 20 seconds.

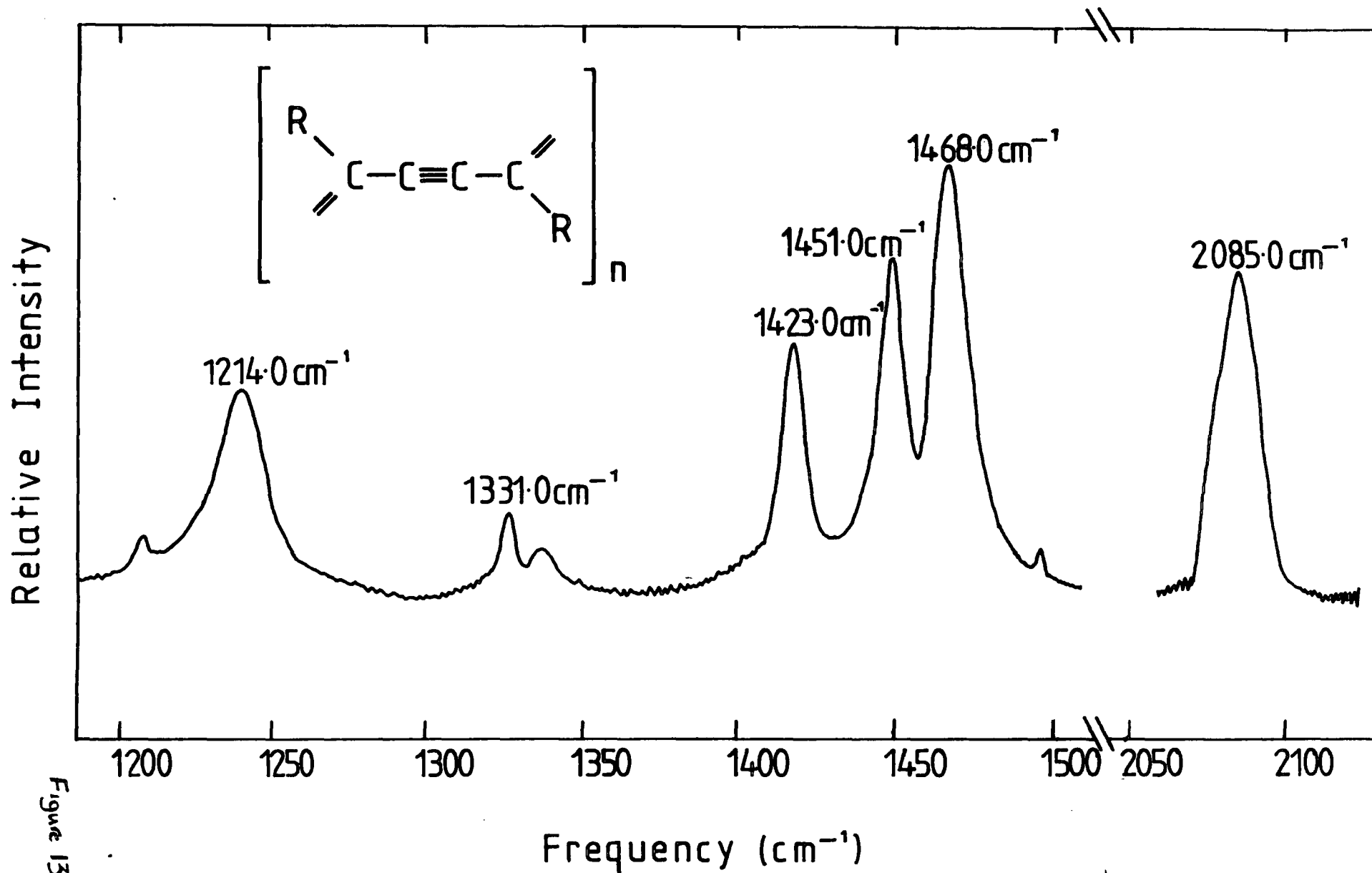
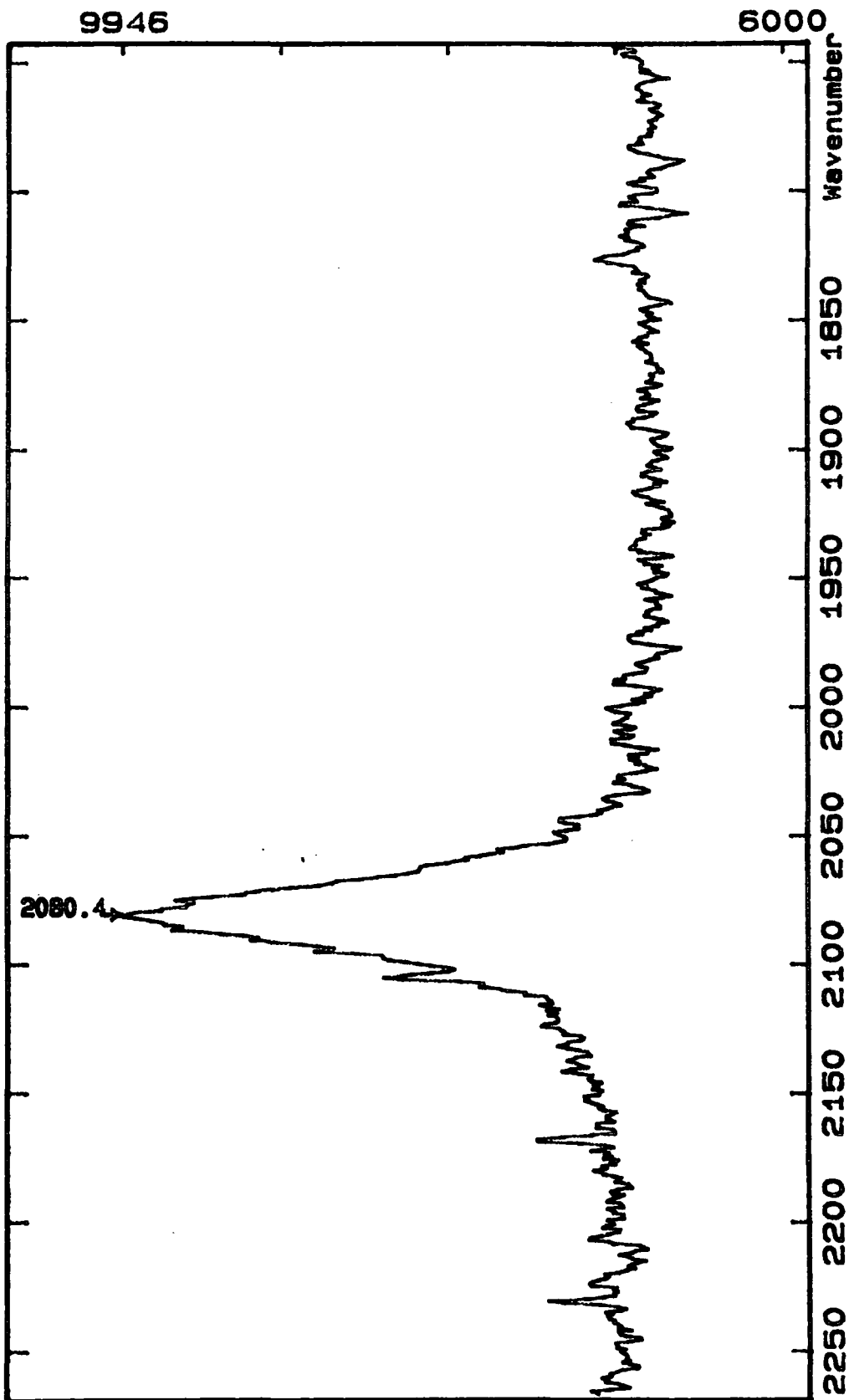


Figure 13

Frequency ( $\text{cm}^{-1}$ )PDA fibre peaks Manufacturers data

\*

poly diacetylene		Ir2443.M50
------------------	--	------------



PEAKS for PDA fibres

Fig 13b

### 3.3 Reproducibility trials

Reproducibility trials were carried out on virgin carbon and glass fibres . the results proved conclusively that it would be illogical to attempt to detect a band shift whilst the glass fibre is in the resin, since there is only a shift of 1 or 2 wave numbers . This kind of variation can normally be expected from fibre to fibre. The only method of obtaining any resonable results would be to look at the fibre end on and this would give only an average value across the entire length of the fibre.

However trials on the pitch based P75 fibres gave good reproducibility with peaks at about  $2189\text{ cm}^{-1}$  and a graphite peak was observed at  $1580\text{ cm}^{-1}$ . Since nylon fluoresce's and shows up in the 2100 and 2200 range. Measurements were made at various points on the fibre. Localised heating due to the laser did not prove to be a problem, in order to prove this the laser was focused on the fibre and a

measurement was made. The laser was left on the spot for 10 minutes after which another measurement was made in which no maximum peak shift was detected.

### **3.4 Single fibre tests**

Single fibre model composites were then subjected to tensile strain and the resulting spectra collected. Prior to this several tests were conducted to determine the effect of localised heating due to the laser on the wave number shift. The laser was focused on one spot for 30, 60, 90 and 120 seconds. There was no change detected in the peak wave number. See figures 14 & 15

Specimens were loaded in tension in 0.1% steps using a miniature testing machine, where one full rotation of the loading wheel was equivalent to 0.075mm cross head displacement. The initial gauge length was 75mm and the data sampling time was maintained at 30 seconds, as an increased

Curve Fitting

Files: Active.....Input:A:NYP.5 .....Output:A:NYP.2CAL  
 Fit: Chi-squared value for last fit..... 184.00  
 Background to peak weighting parameter..... 1.0000  
 Effective peak weighting range (in peak widths).. 1.0000  
 Curves: Number to fit (max 9).....3  
 1.Q/L/G.Q...a0= 124.56 F/XF..a1=0.26235 F/XF..a2=-.24382E-04F/XF  
 2.Q/L/G.L...a0= 50.546 F/XF..a1= 1579.6 F/XF..a2= 14.441 F/XF  
 3.Q/L/G.L...a0= 51.221 F/XF..a1= 1632.7 F/XF..a2= 7.3380 F/XF  
 4.Q/L/G.L...a0=0.00000E+00F/XF..a1=0.00000E+00F/XF..a2=0.00000E+00F/XF  
 5.Q/L/G.Q...a0=0.00000E+00F/XF..a1=0.00000E+00F/XF..a2=0.00000E+00F/XF  
 6.Q/L/G.Q...a0=0.00000E+00F/XF..a1=0.00000E+00F/XF..a2=0.00000E+00F/XF  
 7.Q/L/G.Q...a0=0.00000E+00F/XF..a1=0.00000E+00F/XF..a2=0.00000E+00F/XF  
 8.Q/L/G.Q...a0=0.00000E+00F/XF..a1=0.00000E+00F/XF..a2=0.00000E+00F/XF  
 9.Q/L/G.Q...a0=0.00000E+00F/XF..a1=0.00000E+00F/XF..a2=0.00000E+00F/XF  
 Q=a0+a1\*x+a2\*x^2 G=a0EXP[-((x-a1)/a2)^2] L=a0\*(a2^2)/((x-a1)^2+a2^2)  
 F=Fit a parameter X=fix a parameter  
 Press: F1 to Draw curve, F2 to fit to data,  
 F3 to put into active file buffer, F4 to find background + n-1 peaks.

MESSAGES

FUNCTION KEYS

Keyboard	2	3	4	5	6	7	8	9	0
----------	---	---	---	---	---	---	---	---	---

Active filename: A:NYP.5

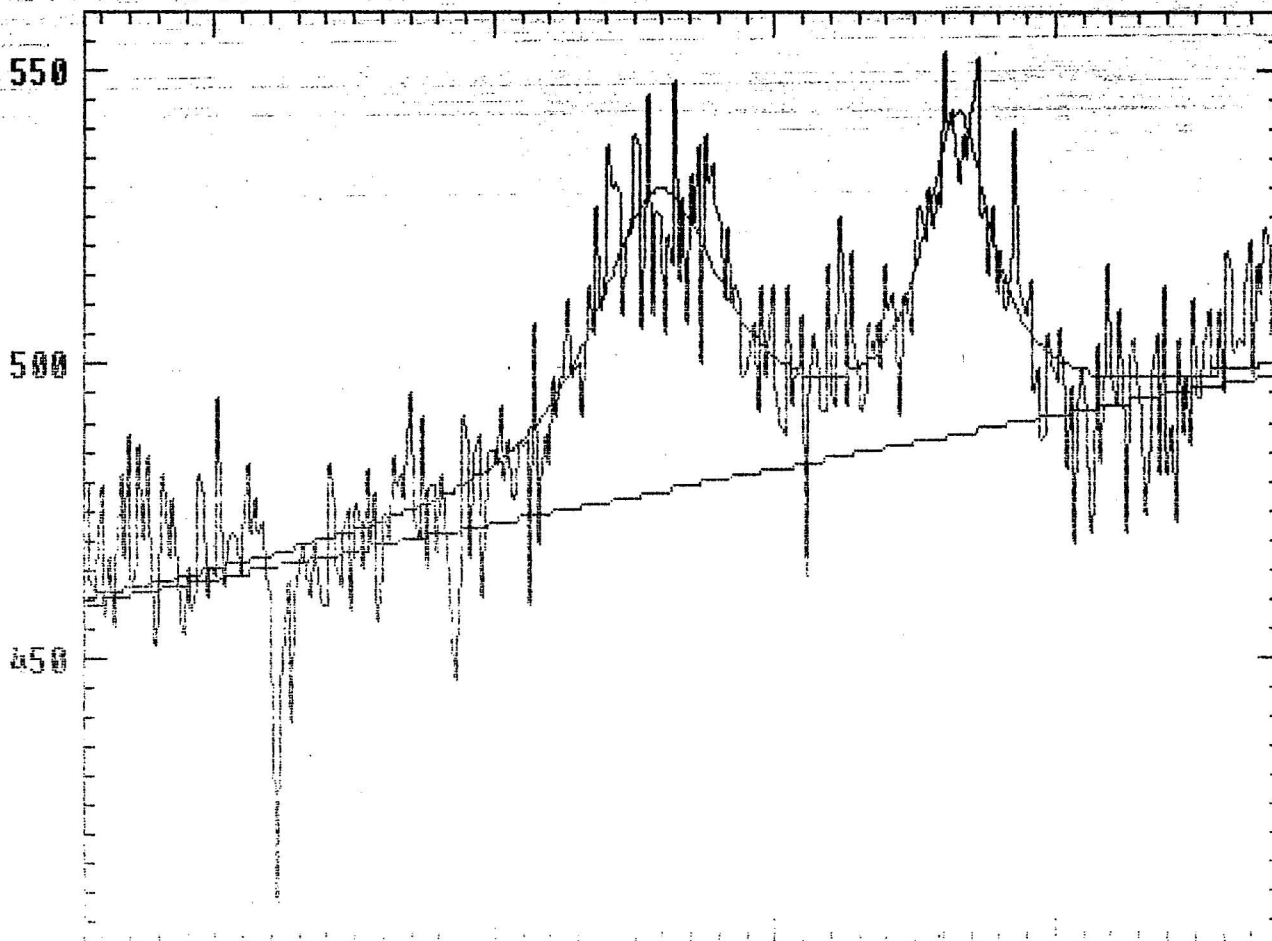


figure 14

Curve Fitting

Files: Active.....Input:A:NPK.4 ....Output:A:PK75.1CAL

Fit: Chi-squared value for last fit..... 2899.6

Background to peak weighting parameter..... 1.0000

Effective peak weighting range (in peak widths).. 1.0000

Curves: Number to fit (max 9).....3

1.Q/L/G.Q...a0= 1437.0 F/XF..a1= 1.8657 F/XF..a2=-.23324E-03F/XF

2.Q/L/G.L...a0= 373.89 F/XF..a1= 1580.7 F/XF..a2= 15.485 F/XF

3.Q/L/G.L...a0= 791.70 F/XF..a1= 1636.3 F/XF..a2= 7.3262 F/XF

4.Q/L/G.Q...a0=0.00000E+00F/XF..a1=0.00000E+00F/XF..a2=0.00000E+00F/XF

5.Q/L/G.Q...a0=0.00000E+00F/XF..a1=0.00000E+00F/XF..a2=0.00000E+00F/XF

6.Q/L/G.Q...a0=0.00000E+00F/XF..a1=0.00000E+00F/XF..a2=0.00000E+00F/XF

7.Q/L/G.Q...a0=0.00000E+00F/XF..a1=0.00000E+00F/XF..a2=0.00000E+00F/XF

8.Q/L/G.Q...a0=0.00000E+00F/XF..a1=0.00000E+00F/XF..a2=0.00000E+00F/XF

9.Q/L/G.Q...a0=0.00000E+00F/XF..a1=0.00000E+00F/XF..a2=0.00000E+00F/XF

Q=a0+a1\*x+a2\*x^2 G=a0EXP[-((x-a1)/a2)^2] L=a0\*(a2^2)/((x-a1)^2+a2^2)

F=Fit a parameter X=fix a parameter

Press: F1 to Draw curve, F2 to fit to data,

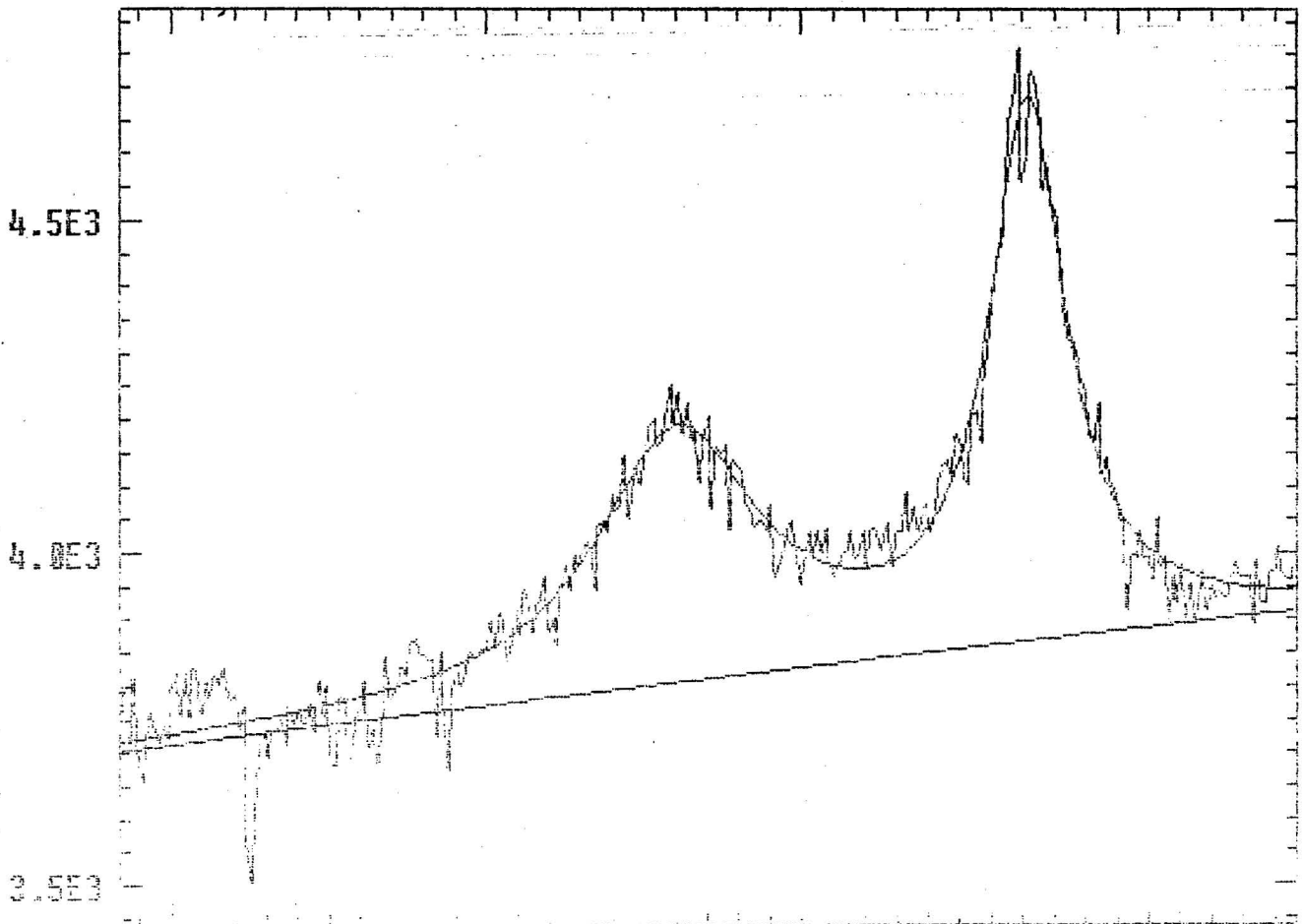
F3 to put into active file buffer, F4 to find background + n-1 peaks.

MESSAGES

FUNCTION KEYS

Keyboard 2 3 4 5 6 7 8 9 0

Active filename: A:NPK.4



figures 15

period had no real benefit to the quality of data obtained. On each occasion the fibre broke at approximately 0.3% strain. This was as expected from previous work and manufacturers data.

**3.4.1 Critical length measurements for certain PA/Fibre systems**

Critical length measurements were made using the Cox model as described in section 6.4 . For simplicity the data is tabulated below.

Material	Fibre Modulus (GPa)	Matrix Modulus (GPa)	Mean Fibre Dia $\mu$	Number average fibre length $\mu$	Critical Fibre Length $\mu$
PA/50%GL	76	2.8	17	1532.47	517
PP/50%GL	76	1.4	17	1532.47	733
PA/50%GL Condition	76	1.4	17	500	733
PA/CF	300	2.8	8	1000	485

Table 1 Critical fibre length obtained form the Cox model

### 3.5 Fibre length distributions

Fibre lengths were measured by image analysis/optical microscopy method (seescan satellite/Olympus stereo microscope) from fibres released from the polymer matrix by pyrolysis on samples 3mm thick. The results are given below

Sample	Skin		Core	
	Num. (mm)	Average	Num. (mm)	average
Long GL/PA MLF		0.71		0.63
Long GL/PA CONV		0.62		0.84
Short GL/PA MLF		0.23		0.23
Short GL/PA CONV		0.23		0.23

**Table 2: Number average fibre lengths (mm) in skin and core regions for all materials in dilatometry study.**

The fibres remaining from pyrolysis of this type of material retain their structure as imposed by the injection moulding process, and as a result the skin and core are easily identified as distinct layers and the fibres may be extracted from each layer with ease. This serves to increase the relative accuracy of the fibre length results and provide morphological information regarding the degree of fibre attrition.

In the case of the long GL/PA, the results indicate that similar fibre lengths are found by both processing routes. This is surprising, since the multiple live feed process reduces the fibre length number average by a factor of two and the percentage volume of fibres in excess of 1mm by a factor of five. For the 3mm thick samples the reduction in fibre length from the multiple live feed samples might be

limited due to the skin formation, essentially limiting the shearing forces proficient due to the packing cycle. Conventional moulded samples exhibit a higher fibre length, indicating a reduced fibre attrition by this method when compared with multiple live feed samples. The number of fibres above 1mm is about 10% of the total for both processing routes, indicating that at a mean fibre volume fraction of 40% in each sample, only 45 of the volume fraction has a length in excess of the critical fibre length for glass fibre/Nylon composites.

Data for short GL/PA samples by both processing routes is the same within experimental error of the measurement. Differences between the two materials ignoring the type of processing route can be clearly seen, with the long GL/PA having a mean fibre length about a factor of three larger than that achieved by the short GL/PA.

### **3.6 Experimental Measurements using Tensile Dilatometry**

Tensile deformation of parallel sided specimens machined from the centre of the coathanger plaque mouldings allowed the measurement of tensile modulus and volume strain for each type of material. The specimen geometry tested had the stress aligned parallel to the mould fill direction. Each specimen had a width of approximately 12.5 mm and a gauge length of 100 mm. The deformation was performed using a screw driven 6025 Instron at a cross head rate of 1 mm/min, with strain measurements being monitored in three mutually perpendicular directions, together with the applied stress. The temperature for testing was held initially at 23°C and some tests were repeated at the higher temperature of 60°C.

The measured values for modulus (taken at 0.2% axial strain), lateral contraction ratios in the width and thickness directions (determined from the slope of the

lateral/axial strain up to 0.5 % axial strain) and the volume strain (determined at 1.0 % axial strain) are shown in the tables below:-

Material	E GPa	LCR (W)	LCR (T)	$\sigma$ (MPa)	Condition
Long PA/GL	15.64	0.37	0.37	195	Dry
MLF	11.36	0.52	0.44	121	Wet 24H
	8.95	0.51	0.40	115	Wet 168H
Short PA/GL	14.69	0.42	0.36	171	Dry
	9.37	0.49	0.38	135	Wet 24H
MLF	6.57	0.50	0.42	90	Wet 168H
Long PA/GL	16.67	0.37	0.36	215	Dry
Conv.	10.62	0.45	0.38	140	Wet 24H
	8.20	0.48	0.48	110	Wet 168H
Short PA/GL	14.75	0.42	0.36	187	Dry
	9.51	0.46	0.38	124	Wet 24H
Conv.	7.00	0.53	0.44	97	Wet 168H

**Table 3: Tensile modulus, width and thickness lateral contraction ratios (all measured at 0.2% applied strain) for all sample types at a thickness of 3mm. The tests were performed at 1 mm/min speed and at 23°C in the dry and conditioned state. The mean results from three specimens are quoted.**

Material	E GPa	LCR (W)	LCR (T)	$\sigma$ (MPa)	Condition
Long PA/GL	15.57	0.39	0.38	145	Dry
MLF	13.30	0.52	0.45	—	Wet 24H
	9.00	0.63	0.49	87	Wet 168H
Short PA/GL	14.51	0.40	0.36	145	Dry
	12.19	0.46	0.39	135	Wet 24H
MLF	6.55	0.49	0.42	88	Wet 168H
Long PA/GL	13.64	0.38	0.33	140	Dry
Conv.	12.62	0.46	0.39	136	Wet 24H
	5.52	0.48	0.60	78	Wet 168H
Short PA/GL	13.52	0.38	0.37	162	Dry
	8.91	0.42	0.41	114	Wet 24H
Conv.	6.98	0.50	0.39	100	Wet 168H

**Table 4: Tensile modulus, width and thickness lateral contraction ratios (all measured at 0.2% applied strain) for all sample types at a thickness of 6mm. The tests were performed at 1 mm/min speed and at 23°C in the dry and conditioned state. The mean results from three specimens are quoted.**

Material	E GPa	LCR (W)	LCR (T)	$\sigma$ (MPa)	Condition
Long PA/GL	11.79	0.49	0.39	152	Dry
MLF	7.57	0.43	0.39	87	Wet 168H
Short	10.65	0.54	0.48	123	Dry
PA/GL	6.39	0.54	0.48	74	Wet 168H
MLF					
Long PA/GL	10.58	0.40	0.41	147	Dry
Conv.	7.21	0.47	0.49	80	Wet 168H
Short	10.63	0.44	0.47	114	Dry
PA/GL	6.24	0.58	0.41	76	Wet 168H
Conv.					

**Table 5: Tensile modulus, width and thickness lateral contraction ratios (all measured at 0.2% applied strain) for all sample types at a thickness of 3mm. The tests were performed at 1 mm/min speed and at 60°C in the dry and conditioned state. The mean results from three specimens are quoted.**

Material	E GPa	LCR (W)	LCR (T)	$\sigma$ (MPa)	Condition
Long PA/GL	11.02	0.48	0.41	88	Dry
MLF	8.10	0.53	0.44	73	Wet 168H
Short	10.08	0.46	0.43	90	Dry
PA/GL	5.24	0.42	0.62	43	Wet 168H
MLF					
Long PA/GL	9.74	0.41	0.38	131	Dry
Conv.	5.52	0.41	0.70	54	Wet 168H
Short	10.62	0.44	0.47	114	Dry
PA/GL	6.24	0.58	0.41	76	Wet 168H
Conv.					

Table 6: Tensile modulus, width and thickness lateral contraction ratios (all measured at 0.2% applied strain) for all sample types at a thickness of 6mm. The tests were performed at 1 mm/min speed and at 60°C in the dry and conditioned state. The mean results from three specimens are quoted.

The difference in moduli for the two compounds are principally due to the volume fraction differences in the feedstock. The Dispersed compound had a mean fibre volume fraction of 32%, the Undispersed compound had a mean fibre volume fraction of 43%. The mean modulus values for the two compounds reflect these ratios, with the higher volume fraction leading to a higher mean modulus.

There is a clear difference in the value for the width and thickness lateral contraction ratios for each of the compounds. This is to be expected from the microstructure of both compounds. The values for the lateral contraction ratios for the Dispersed and Undispersed compounds in the width direction are the same within experimental error. The thickness lateral contraction ratios for the Dispersed and Undispersed compounds are different; this is due to slight variations in the microstructure in the materials.

These values for the lateral contraction ratios can be used to estimate the volume strain-axial strain function. The predicted values for the volume strain at 1.0% applied axial strain are shown below:-

Compound Type	$V_s$ Predicted ( $\epsilon = 1.0\%$ )	$V_s$ Measured ( $\epsilon = 1.0\%$ )
Long GL/PA MLF	0.26	
Long GL/PA Conv	0.22	
Short GL/PA MLF	0.27	
Short GL/PA Conv	0.22	

**Table 7: Predicted versus measured volume strain response at 1.0% applied strain for all the materials.**

The predicted result for the Dispersed compound is in good agreement with the measured mean value for the volume strain, indicating that the deformation up to 1.00 % applied strain is primarily dilational in nature. For the Undispersed compound, the predicted result is somewhat smaller than the measured mean value for the volume strain. This indicates that an extra volume increasing mechanism is occurring over the strain range considered. The likely candidate is some form of cavitation, which might include debonding at the fibre matrix interface and an increase of voiding due to poorly wetted areas of the compound. The volume strain plot for the dispersed compound follows the predicted line. The volume strain-axial strain plot for the Undispersed compound shows departure from the predicted line at about 0.5 - 0.8% axial strain. This indicates that a cavitation type process begins at this value of deformation.

#### **4 Torsional and Flexural stiffness of long/short fibre nylon composites.**

Torsional creep experiments were carried out on the apparatus as represented schematically in figure 16 . Specimens were in the form of parallel sided strips having a thickness of 3mm. Specimens were loaded in steps of 20g up to 120g, the cycle being 100 seconds under load 600 seconds recovery, the deflection after each time period being noted.

Figures 17, 18, 19 & 20 show the data for dry and conditioned, multi-live feed and conventional specimens.

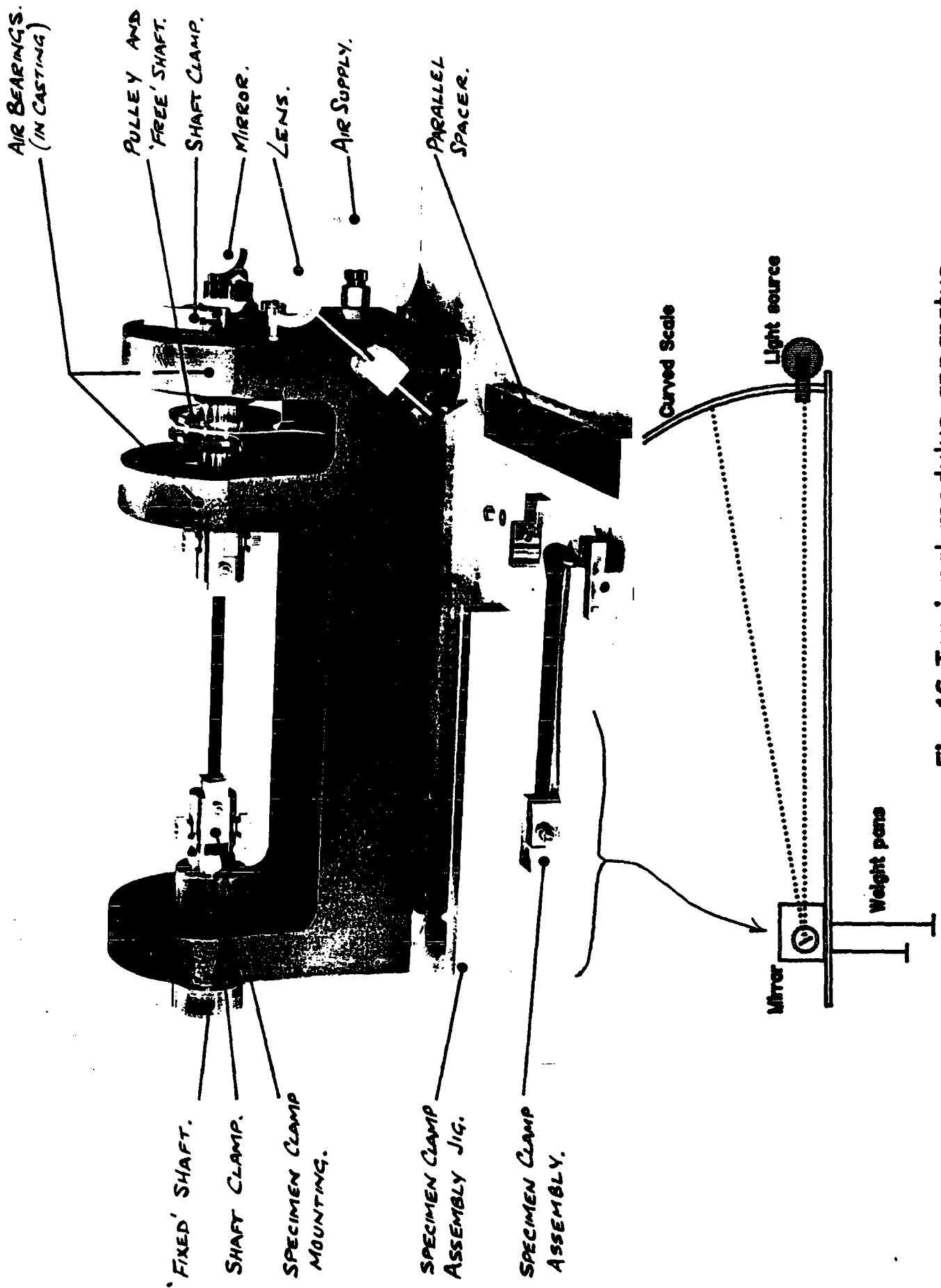
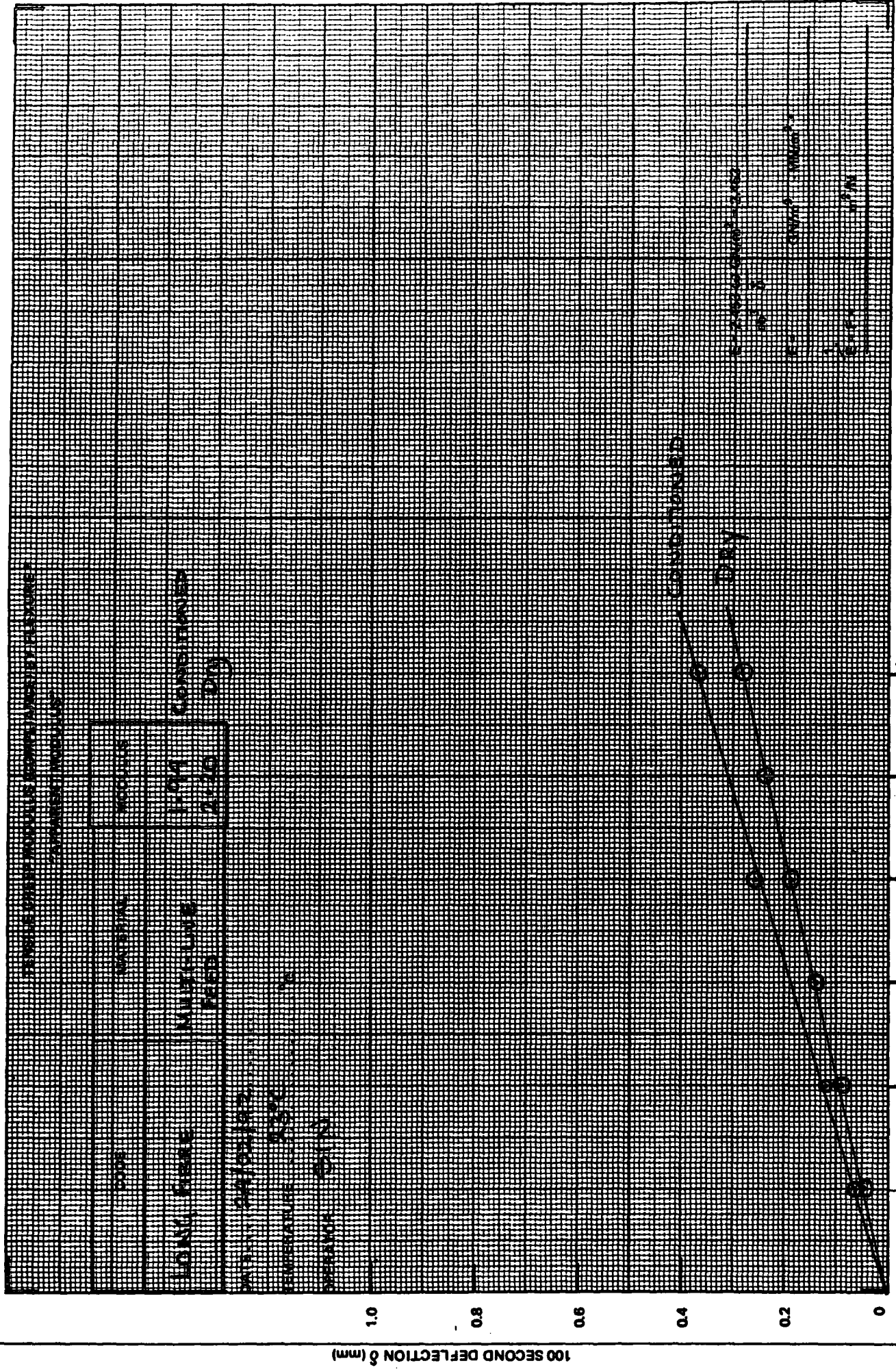


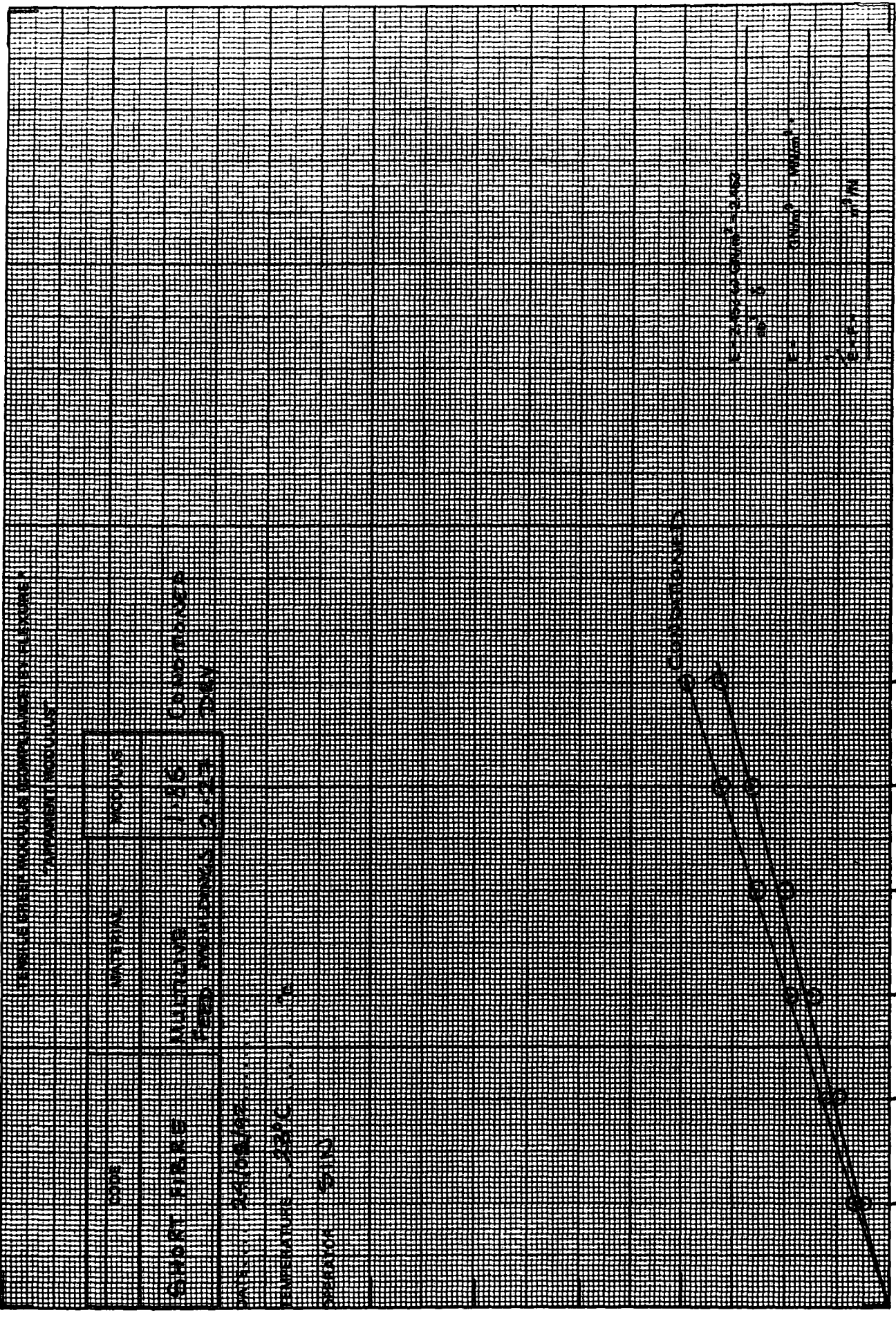
Fig 16 Torsional modulus apparatus



TESTING INSTRUMENTS COMPANY, WESTLEY, MASSACHUSETTS

DATE	TESTER	TESTING
10/11/55	MURPHY	1197
10/11/55	1197	CONSTANT
10/11/55	1197	CONSTANT

10/11/55  
 1197  
 1197

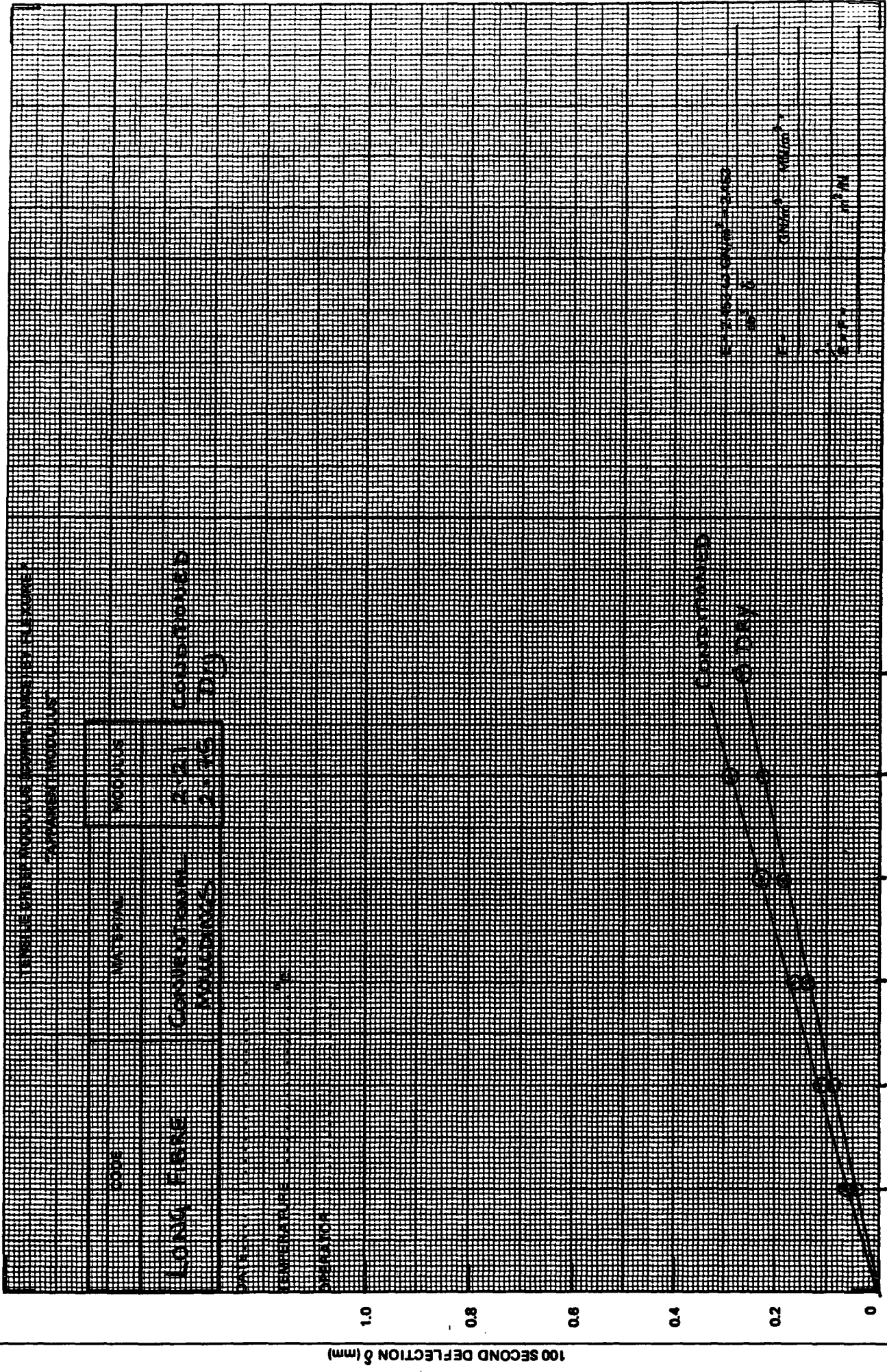


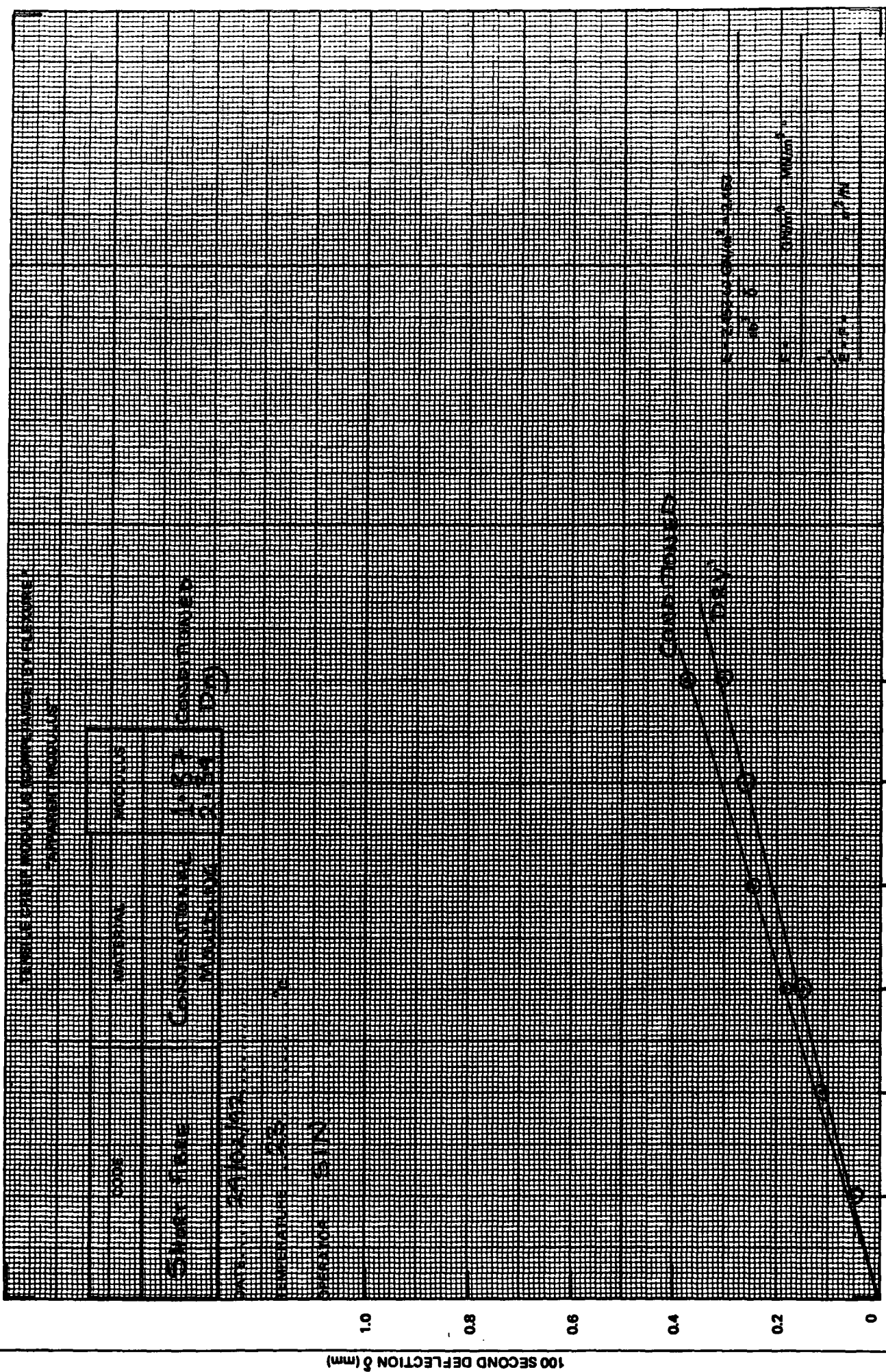
TESTING MACHINE MODEL NO. 100  
 SERIAL NO. 100

LOAD	DEFLECTION
0	0.00
20	0.15
40	0.30
60	0.45
80	0.60
100	0.75
110	0.78
120	0.80

100 SECOND DEFLECTION (mm)

LOAD (g)





LOAD	DEFLECTION
0	0
20	0.05
40	0.10
60	0.15
80	0.20
100	0.22
120	0.23
140	0.24
160	0.25

100 SECOND DEFLECTION  $\delta$  (mm)

LOAD  $\delta$  (kg)

Material	G GPa 3 mm thick	Condition
Long PA/GL MLF	2.35 1.87	Dry Wet 24H
Short PA/GL MLF	2.27 1.86	Dry Wet 24H
Long PA/GL Conv.	2.52 1.94	Dry Wet 24H
Short PA/GL Conv.	2.75 2.20	Dry Wet 24H

**Table 8: Torsional modulus data for dry and conditioned materials.**

Material	E GPa 3 mm thick	E GPa 6 mm thick	condition	E GPa 3mm thick. Wet
Long PA/GL MLF	11.26 (0.48)	11.86 (0.47)	Dry	8.13 (1.0)
Short PA/GL MLF	10.70 (0.51)	13.13 (0.53)	Dry	7.51 (0.9)
Long PA/GL Conv.	11.16 (0.38)	12.52 (0.33)	Dry	7.93 (0.95)
Short PA/GL Conv.	10.84 (0.31)	12.16 (0.41)	Dry	7.87 (0.55)

**Table 9: Flexural modulus data for 3mm/6mm glass/PA composites.**

Material	E (GPa) (23°C)	E (GPa) (60°C)	Condition
Long PA/GL	15.64	11.79	Dry
MLF	8.95	7.57	Wet 168Hrs
Short PA/GL	14.69	10.65	Dry
MLF	6.57	7.57	Wet 168Hrs
Long PA/GL	16.67	10.58	Dry
Conv.	8.20	7.21	Wet 168Hrs
Short PA/GL	14.75	10.62	Dry
Conv.	7.00	6.24	Wet 168Hrs

Table 10: Tensile modulus at 0.25% for 3mm thick specimens.

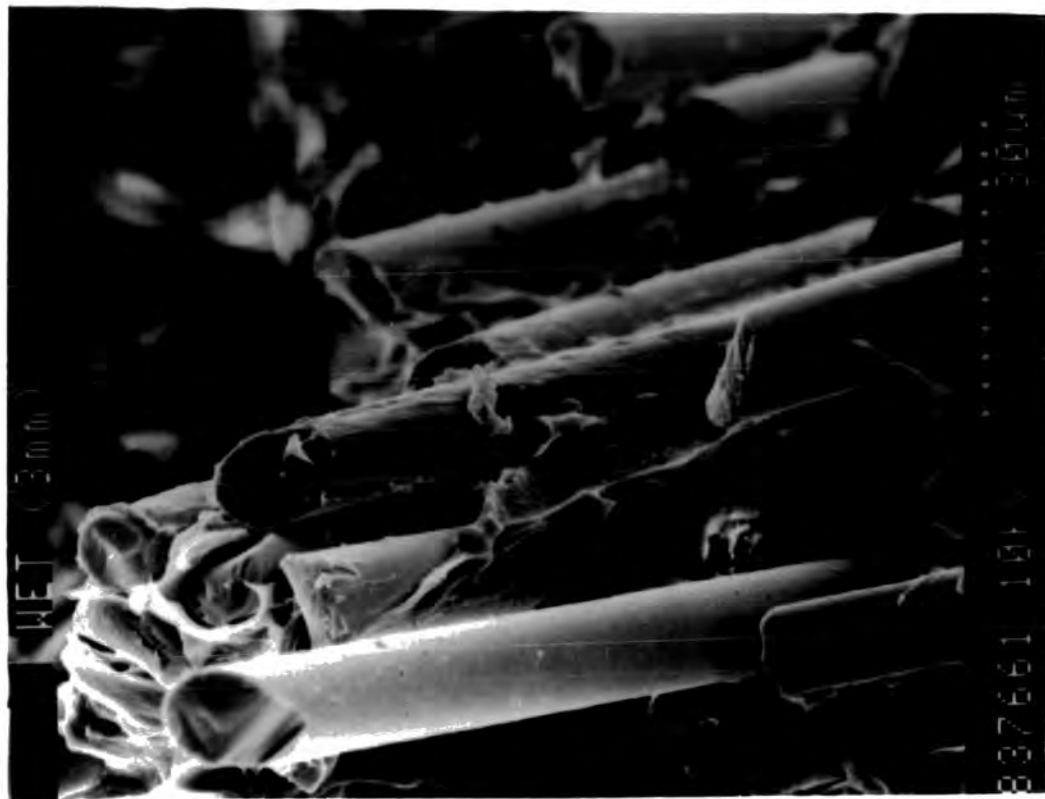
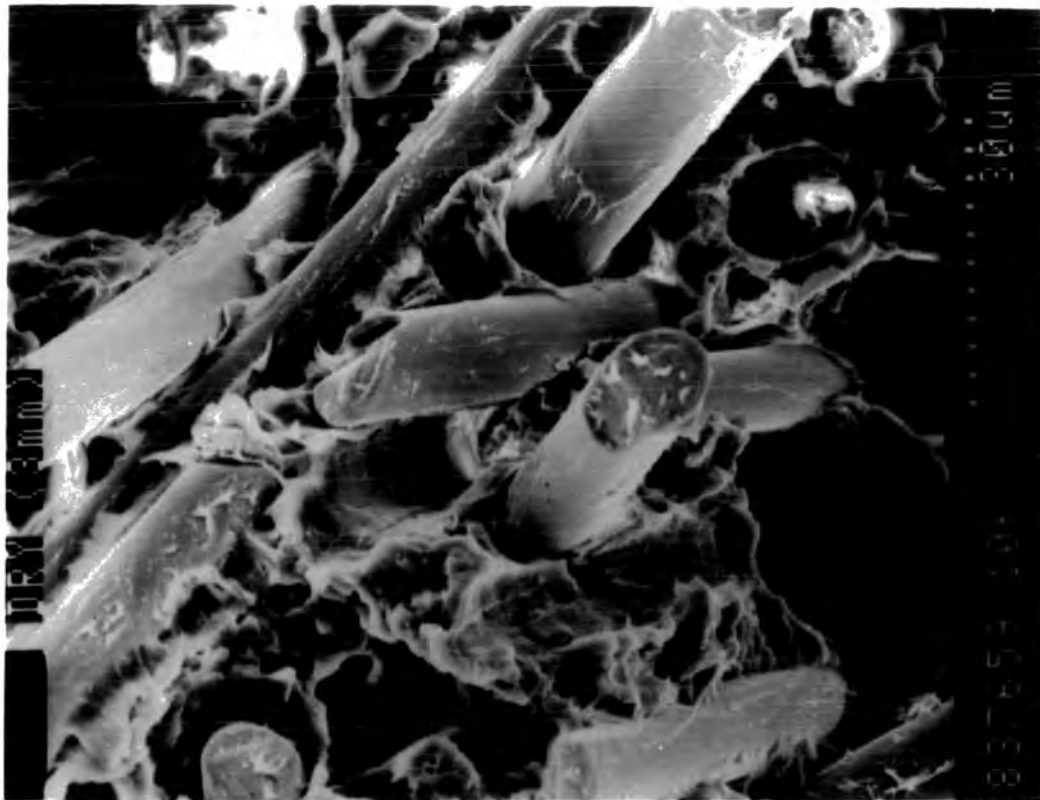


Fig 21 Short glass fibre/PA Tensile dilatometry sample  
a) conditioned 24hrs @ 95C in water  
b) Dried in Vac oven for 24hrs @ 75C.



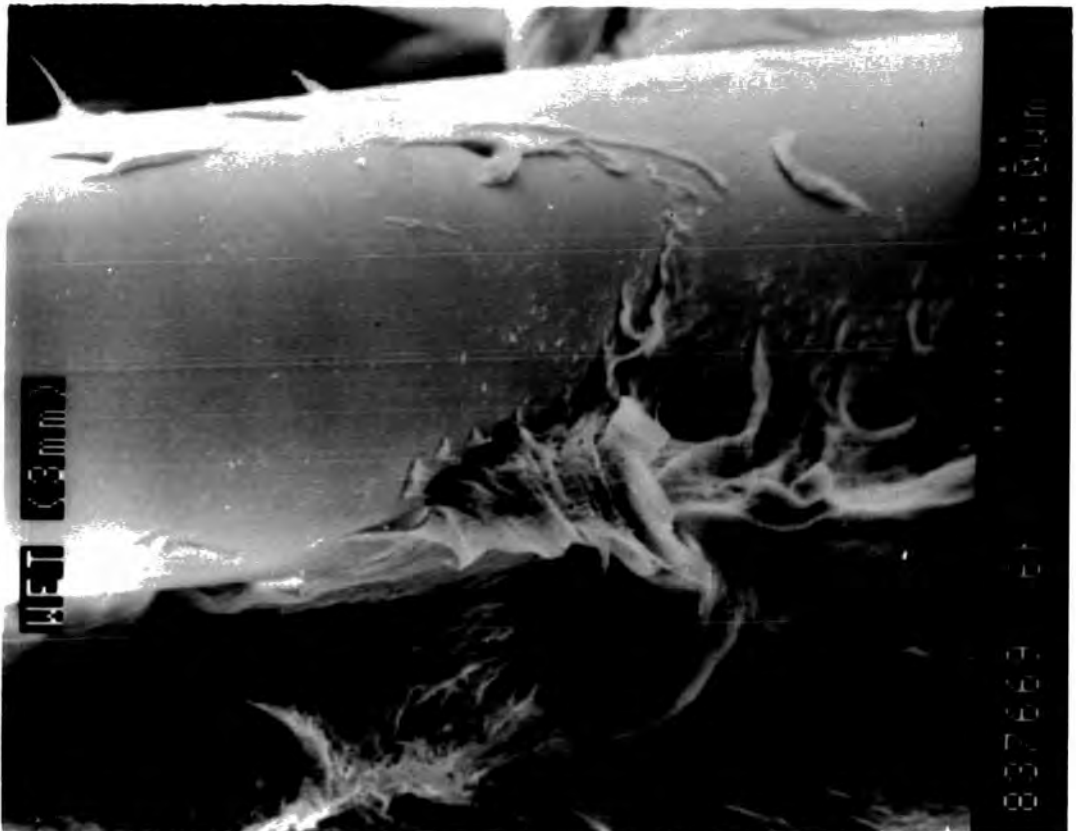
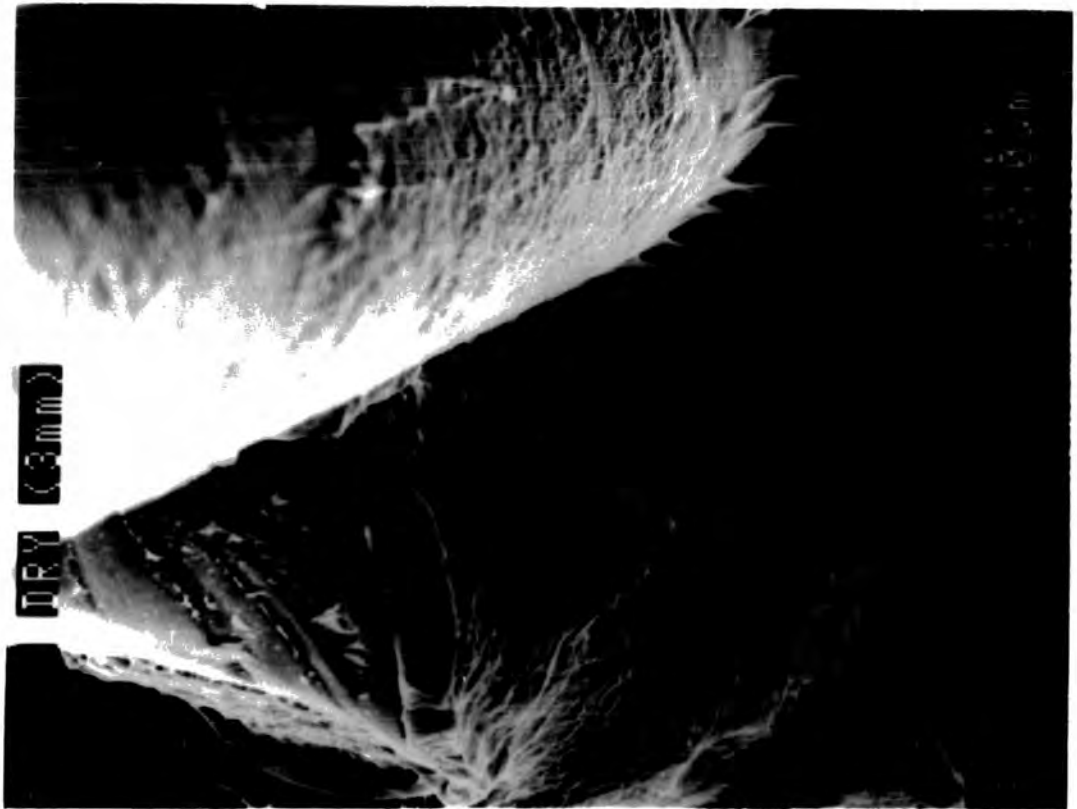


Fig 22 Long glass fibre/PA Tensile dilatometry sample  
a) conditioned 24hrs @ 95C in water  
b) Dried in Vac oven for 24hrs @ 75C.

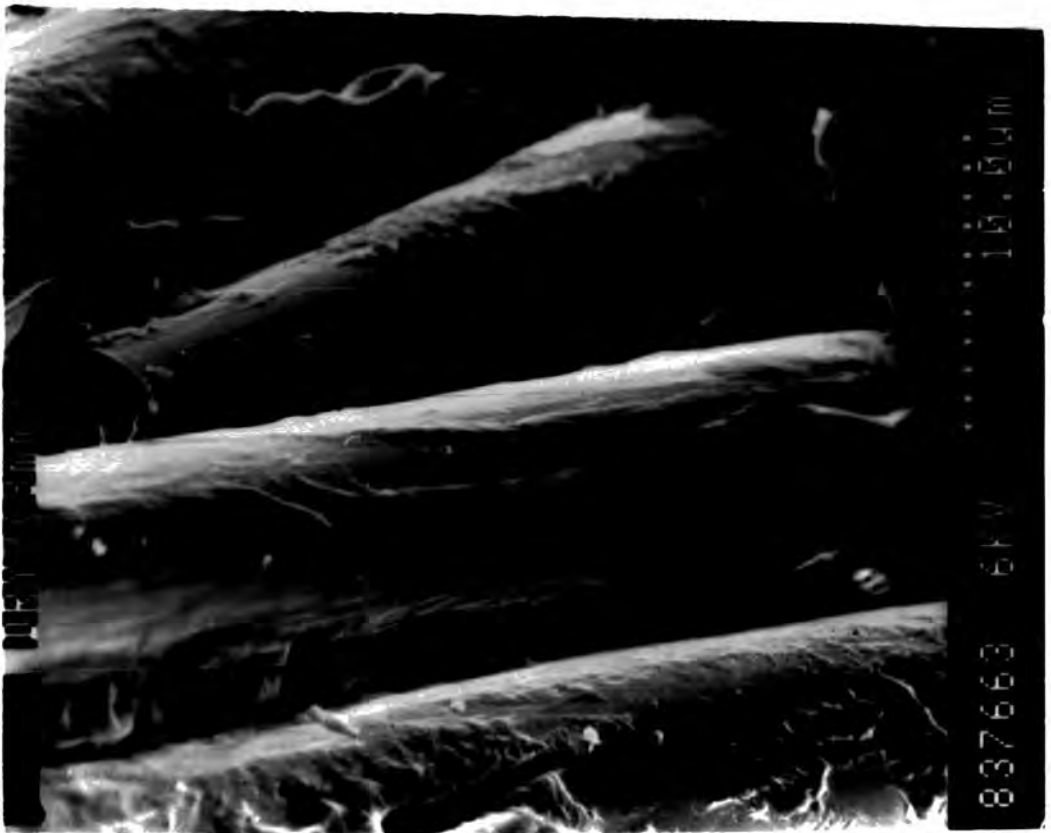
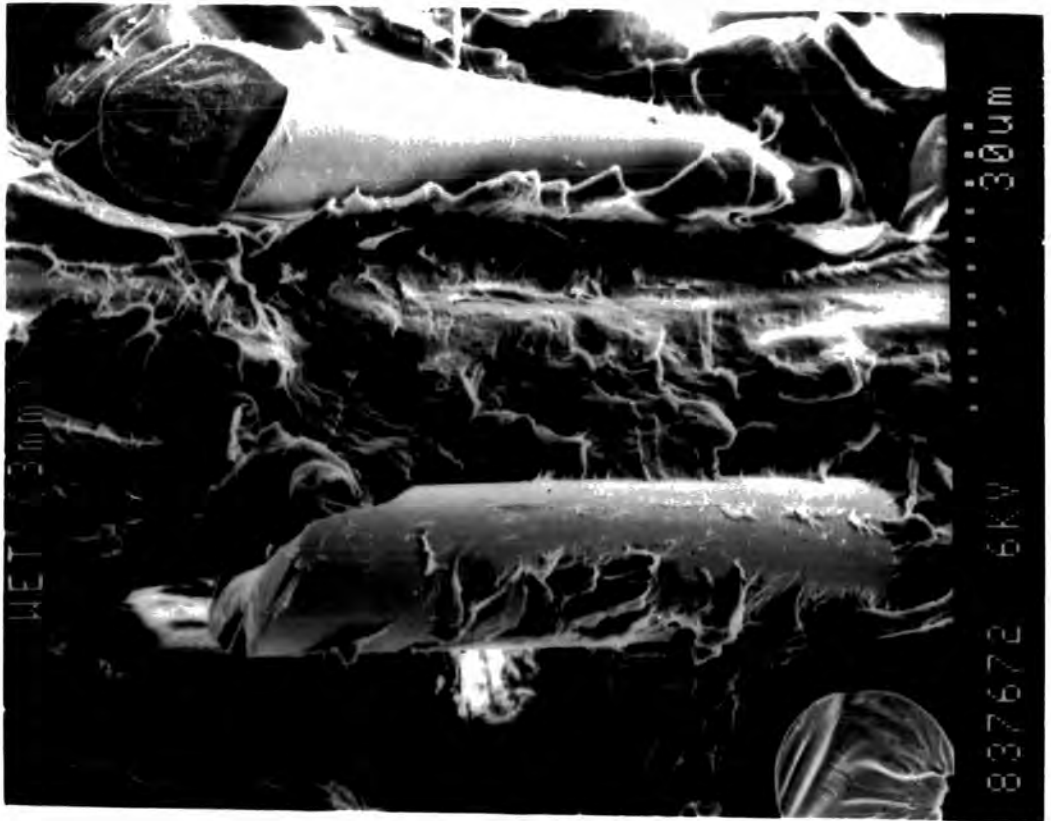


Fig. 23 Interface badly degraded by moisture conditioning leaving clean fibre surfaces(a)  
b) PA matrix adhering to fibre surface on unconditioned specimens

## 5 Discussion and Conclusions

### Tensile Dilatometry

The predicted result for the long fibre MLF and CON and the short fibre CON mouldings is in good agreement with the measured mean value for the volume strain, indicating that the deformation up to approximately 1.00 % applied strain is primarily dilational in nature in both the dry and conditioned states. For the short fibre MLF mouldings, the predicted result is somewhat smaller than the measured mean value for the volume strain. This indicates that an extra volume increasing mechanism is occurring over the strain range considered. The most likely explanation is some form of cavitation such as debonding at the fibre/matrix interface which will increase as the interface breaks down further under moisture attack, leaving the debonded fibres free to slide within their cavities. See Figures 21, 22 & 23. Voiding at the fibre ends may be a contributory factor.

The width and thickness contraction ratios are seen to fall from 0.37 for both fibre types in the dry MLF mouldings to 0.5 and 0.44 respectively after conditioning. A value of 0.5 indicates a rubbery compound and as described previously the mechanical properties of nylon deteriorate with increasing moisture uptake.

The length of the fibre in a moulding relative to the critical fibre length is an important criterion in assessment of both stiffness and strength properties. When the average fibre length is greater than the critical length, then the fibres carry a greater proportion of the applied force. This leads to the fibres reinforcing the matrix material and the composite is therefore stiffer and stronger than the matrix. This process becomes dominant when the average fibre length exceeds the critical fibre length. There was also good comparison between the values obtained for critical length from Cox model and fragmentation tests.

The critical fibre length for the long fibre CON mouldings was estimated using the Cox model and the following results were obtained;

Fibre modulus  $E_f = 76$  (GPA)

Matrix modulus  $E_m = 2.8$  (GPA)

Mean Fibre diameter  $d = 17\mu$

Composite contraction ratio = 0.4

Number average fibre length =  $1532.47\mu$

Critical fibre length  $l_c = 517\mu$  for dry compounds

Critical fibre length  $l_c = 733\mu$  for conditioned compounds.

In order for the composite to be effective in load bearing application the average fibre length in moulded components has to be greater than the critical length. In the case of the short fibre CON mouldings. The number average fibre length is greater than the critical fibre length.

During the Multi-live feed injection process the fibres lengths are reduced further by the shearing process. This could go some way into explaining the fall in properties when comparing long fibre MLF with long fibre CON, with break stress values of 195MPa and 210MPa respectively.

Certain of the properties that have already been described rely on this principle more than others. For example, when the level of deformation is relatively high, then the balance between fibre length and critical fibre length becomes more important. Higher levels of deformation have been noted at test conditions of greater strain, longer times under load, static rather than dynamic loading and higher temperatures. Therefore a number of property comparisons for the long versus the short fibre reinforced composite can be explained by the longer average fibre length compared to its critical fibre length. This includes:-

Greater stiffness at larger strains.

Greater stiffness at longer times under load.

Greater stiffness at higher temperatures.

Higher strength for static loading rather than fatigue loading.

Greater static strength at higher temperatures.

The stiffness of the 23°C results at small strains favoured the short fibre composite. The predicted modulus calculations declared this as no surprise, because the combination of fibre properties and microstructure precipitated such an observation. It has been noted that the consequence of the processing conditions, at least in terms of mould geometry and melt stress fields, result in the different microstructures for these two materials.

The differences in flexural properties are to be expected since Flexural modulus is usually smaller than tensile modulus. The flexural modulus for both moulding types is

approximately equal indicating a small effect of the skin core.

Shear modulus  $G$ , of the conventional mouldings is greater than that of multi-live feed mouldings, this could in part be due to the effect of the skin core. As a consequence  $G$  for the composite falls as the matrix  $G$  falls with conditioning.

The shear modulus of nylon falls with humidity and the fall of the shear modulus of the composite with increasing humidity falls as a function of the shear modulus of nylon.

How then can a judgement be made on which material might concede the better mechanical behaviour in stiffness or strength performance of a component? The following answers might be proposed for discontinuous fibre reinforced engineering thermo-plastics:-

(i) If a singular choice emerges from a limited evaluation, then the chances of it being either correct or even optimum

are not good.

(ii) It is likely that a balance of in-service conditions relating to various stress conditions would favour the longer fibre reinforced system.

(iii) A universal view of the mechanical performance of the materials should embrace more than one geometry of component.

Obviously, a more detailed understanding of processing and resultant properties will lead to better design with these materials.

## 6 REFERENCES

1 Holister & Thomas " Fibre reinforced materials" Elsevier Publishing co, London, 1966.

2 PRI " Deformation and fracture of composites" 1st Int. Conf. UMIST, Manchester, March 1991.

3 SW Tsai. " Composites design" 4th edition, Think composites, Dayton, OHIO, 1988

4 Hull D. " Introduction to composite materials". Cambridge University press, Cambridge UK 1981

5 Kelly A, Tyson WR. " Tensile properties of fibre reinforced metals ". J.Mech.Phys.Solids 13 1965

6 Kodokian KA, Kinloch AJ. "Surface pretreatment and adhesion of thermo-plastic fibre composites." J Mat.Sci Letters 1988 (625-627).

7 Peacock JA, B Fife, " Composite interfaces" edited by Ishida H and Koenig JL N York 1986 (146)

8 Broutmann LJ " fibre matrix interactions" Poly.Comps. Oct 1982 Vol3 (179)

9 Ehrburger P, Herque J, Donnet JB "Electrochemical treatment of carbonfibres" 4th London conference, Soc.Chem.Industr. 1976 (190)

10 Molleyre F and M Bostick. 4th London Conference, Soc.Chem.Industr 1976 (190)

11 Fitzer E, Geigl KH and Manocha LM . 5th London intercarbon

graphite. Soc.Chem.Industr 1978 (405)

12 Goan JC, Joo LA, Sharpe GE. "Surface treatment for graphite fibres" Proc. 27th An.Tech.Confr. 1972

13 Ehrburger P and JB Donnet. " Interface and composite materials". Phil.trans R. Soc London A294 1980 ( 495-505)

14 Pinchin DJ, Woodhams RT. " Pyrolytic surface treatment of graphite fibres ". US patents 4,130,495 Dec 1978

15 Broutmann LJ, Agarwal BD." A theoretical study of the effects of interfacial layer on the properties of composites". Poly.Eng.Sci. 14/8 581 1974

16 Broutmann LJ, Agarwal BD. " A theoretical study of the effects of interface on composite toughness". Proc.28th Ann.Tec.Conf Sept 1973.

17 Di-Benedetto AT, Nicholais. " Interface in composites". Advnc.Comp.Matrl. Ch 8 Applied sci. pub/ 1978.

18 Lavengood RE, Michno MJ ." The effects of thick interlayers on the mechanical performance of the fibre reinforced composites ". SPE-EPS Division Tech Conf. Additives 1973.

19 Hancox NL, Wells H." Effects of fibre surface coatings on the mechanical properties of CFRP". Fibre Sci.&.Tec 10 1977

20 Atkins AG." Impact strength of thick interlayer composites". Journal.Appl.Poly.Sca.

21 Rasen BW. " Tensile failure of fibrous composites ". AIAA  
C2 No. 11 1969

22 Cox HL. "The elasticity and strength of paper and other  
fibrous materials". Brit Jor.App.Physics. 1952.

23 Dow NF. " Study of stresses near a discontinuity in a  
filament reinforced composite metal" . GEC TIS R635D61 1963.

24 Broutmann LJ. "Measurement of the fibre=polymer matrix  
interfacal strength" Interfaces in composites Conf. ASTM  
STP 452 1969.

25 P Lawrence." Some theoretical considerations of fibre  
pull out from an elastic matrix ". J.Matl.Sci. 1972.

26 Bartois P. " Analysis of pullout tests on fibres embedded  
in brittle matrices ". J.Matl.Sci. 1972.

27 Greszczuk LB " Theoretical studies of the mechanics of the fibre/matrix interface in composites ". Interfaces in composites ASTM STP 452 Am.Soc.materials testing 1969.

28 Pitkethley MJ Doble LB." Evaluating the maximum bond shear strength of a fibre resin interface using a single fibre pull out technique ". IPCM 1989 Sheffield university

29 Penn LS Lee SM." Interpretations of experimental results in the single filament pull out test ". J.Comp.Tech.&.Res. Vol 11 1989.

30 Outwater OJ & Murphy MC." The fracture energy of unidirectional laminates ". 24th Ann. Tech.Conf. 1969

31 Outwater & Murphy. " The influence of environment and glass finish on the fracture energy of glass epoxy joints ". 25th Ann.Tech.Conf.1970.

32 A Kelly. " The strengthening of metals by dispersed particles". Proc,Royal.Soc 19282 63 1984

33 McGarry FJ & Fujiwara." Resin fibre load transfer in reinforced plastics ". Modern Plastics. July 1968

34 Fraser WA, Ancker FH & Di Benedetto." Computer modelled single fibre technique for measuring coupling and sizing agent effects in fibre reinforced composites ". 30th Ann.Conf. Of SPI 11A 1972

35 Origchin L, Olender & Ancker FH." Fibre matrix adhesion and the fracture behaviour of Glass reinforced high density polyethylene". 27th Ann.Tec.Con. 1972.

36 Ishikawa M, Nuvishawa I & Ogwa." A study of the interlaminar shear fracture in carbon fibre composites ". Yamaguta University.

37 Drzal LT, Rich MT & Hall. " Structure property relationships at the composite interfaces ". 15th Bi.ann conf.carbon.USA Carbon society 1981.

38 Di-Benedetto HT Nicholais L. " Technique for evaluating the effects of coupling agents on the strength of interface in fibre composites". 40th Ann. Tech.Conf. 1895

39 Pe McMahon and L Ying. " Effect of fibre matrix interactions of the properties of graphite/epoxy composites". NTIS report N83-10120 1983

40 Robinson IM. " Optomechanics of single fibre composites" M.Phil-Ph.D transition report. QMWC, London university.

41 Naqui SI, Robinson IM. "A review of tensile dilatometric studies of deformation in polymeric materials and their composites" Accepted for publication Journal Materials



Science Jan 1992